

MODELING OF THE HUMAN HEAD/NECK SYSTEM  
USING RIGID BODY DYNAMICS

by

Christina Renee Estep

Thesis Submitted to the Faculty of the  
Virginia Polytechnic Institute and State University  
in partial fulfillment of the requirements for the degree of  
MASTER OF SCIENCE  
in  
Engineering Mechanics

APPROVED:

Daniel J. Schneck

D. J. Schneck

S. L. Hendricks

S. L. Hendricks

I. Kaleps

I. Kaleps

July, 1992

Blacksburg, Virginia

LD  
5655  
V855  
1992  
E874

MODELING OF THE HUMAN HEAD/NECK SYSTEM  
USING RIGID BODY DYNAMICS

by

Christina R. Estep

Committee Chairman: Dr. Daniel Schneck  
Engineering Science and Mechanics

(ABSTRACT)

Emergency ejection of an air crew member from military aircraft in flight places dangerously large vertical acceleration forces on the body of the member. The additional mass on the head due to Night Vision Goggles and Helmet Mounted Displays increases the vulnerability of the head/neck system to injury. To eliminate the need for human testing, computer simulations of biodynamic head and neck system response to large vertical accelerations have been produced. A head/neck characteristic was developed which included the rotation and axial deformation properties of the cervical spine. The characteristic consisted of three rigid segments representing the head, neck, and upper torso, a ball-and-socket joint representing the head/neck articulation, and a slip joint representing the neck/torso articulation. The model was exercised using the Articulated Total Body Model developed by Calspan Corporation and Armstrong Laboratory. The model parameters were determined using human vertical deceleration test data acquired at Armstrong Laboratory. Simulations of human biodynamic response to ejection

acceleration show the proposed head/neck characteristic to produce improved correlation with human biodynamic response to 10 G<sub>z</sub> acceleration when compared to previous rigid body models of the human head/neck system.

# Acknowledgements

The author wishes to express her appreciation for the financial support of Systems Research Laboratories under Contract F33615-89-C-0574 DO-C9. The technical support of Dr. Scott Hendricks at VPI&SU, and Dr. Ints Kaleps and the individuals at Armstrong Laboratories is also appreciated. The author is grateful to Dr. Daniel Schneck for his advice and technical support which was invaluable for the fruition of the project.

# Table of Contents

| <u>Chapter</u>   | <u>Page</u> |
|--|-------------|
| List of Tables.....  | vii         |
| List of Figures.....   | viii        |
| List of Symbols.....   | x           |
| 1.0 Introduction.....  | 1           |
| 2.0 Literature Review.....   | 6           |
| 3.0 Operational Background of the ATB Model.....                             | 17          |
| 3.1 General Formulation of the ATB Model.....                                | 17          |
| 3.2 System Equations.....  | 23          |
| 4.0 Problem Statement and Formulation.....                                   | 29          |
| 4.1 Anatomical Description of the Head and Neck.....                         | 29          |
| 4.2 Computer Model of the Head and Neck.....                                 | 36          |
| 5.0 Solution Methods.....  | 44          |
| 5.1 Live Human Subject Ejection Simulations.....                             | 44          |
| 5.2 Computer Ejection Simulations with Current ATB<br>Head/Neck Analog.....  | 55          |
| 5.3 Computer Ejection Simulations with Proposed ATB<br>Head/Neck Analog..... | 66          |
| 6.0 Results and Discussion.....  | 72          |
| 7.0 Summary and Conclusions.....   | 84          |

7.1 Modeling of the Head and Neck..... 84

7.2 Direction of Future Studies..... 86

**8.0 References..... 88**

**Appendices.....91**

# List of Tables

| <u>Table</u>  | <u>Page</u> |
|---|-------------|
| 5.1 Anthropometric Data for Subject L7.....           | 53          |
| 5.2 Joint Flexure Spring Coefficients.....            | 64          |
| 5.3 Viscoelastic Spring and Damping Coefficients..... | 70          |



# List of Figures

| <b><u>Figure</u></b>   | <b><u>Page</u></b> |
|--|--------------------|
| 1.1 Test Configuration for Seated Human Subject<br>with Added NVG/Helmet Combination.....  | 2                  |
| 2.1A Comparison of Kaleps' Simulated and Experimental<br>Resultant Chest Acceleration During 10 G Peak<br>-G <sub>x</sub> Impact.....                | 8                  |
| 2.1B Comparison of Kaleps' Simulated and Experimental<br>Resultant Head Acceleration During 10 G Peak<br>-G <sub>x</sub> Impact.....                 | 8                  |
| 2.2 Becker's Head/Neck System Joint Forcing Elements....   | 10                 |
| 2.3 Comparison of Frisch and Cooper's Simulated and<br>NAMRL Experimental Head Angular Acceleration During<br>9.8 G Peak -G <sub>x</sub> Impact..... | 12                 |
| 2.4 Forcing Functions for Freivalds and Kaleps<br>Muscle Model.....  | 14                 |
| 3.1 Standard ATB 15 Segment/14 Joint Model of<br>the Human Body.....   | 19                 |
| 3.2 Inertial, Local, and Joint Coordinate Systems of<br>the ATB Head/Neck Model.....   | 20                 |
| 4.1 Anatomical Representation of the Human<br>Head/Neck System.....  | 30                 |
| 4.2 Motions Involved in Head Movement.....   | 32                 |
| 4.3 Three Segment/Two Ball-and-Socket Joint Model<br>of Head/Neck System.....  | 37                 |
| 4.4 ATB Model Joint Spring, Coulomb, and Viscous<br>Restoring Torque Functions.....  | 39                 |
| 5.1 Armstrong Laboratory's Vertical Deceleration Drop<br>Tower.....  | 45                 |

|      |  |    |
|------|--|----|
| 5.2  | Accelerometer Coordinate System for Vertical<br>Deceleration Drop Tower Test.....  | 47 |
| 5.3  | Measured Carriage Acceleration for Human<br>Drop Tower Test.....   | 48 |
| 5.4  | Measured Subject Chest Acceleration for Human<br>Drop Tower Test (Filtered of 50 Hz and Above).....  | 50 |
| 5.5  | Measured Subject Head Acceleration for Human<br>Drop Tower Test (Filtered of 50 Hz and Above).....   | 51 |
| 5.6  | Anatomical Coordinate System for Human Head.....   | 54 |
| 5.7  | Subject Mounted Fiducial Location for Human<br>Test Photogrammetric Data.....  | 56 |
| 5.8  | Test Subject Chest Photogrammetric Data.....   | 57 |
| 5.9  | Test Subject Head Photogrammetric Data.....  | 58 |
| 5.10 | Physical Measurements of Human Head/Neck Model.....  | 60 |
| 5.11 | Three Segment/Ball-and-Socket and Slip<br>Joint Viscoelastic Head/Neck Model.....  | 67 |
| 6.1  | Response of Original ATB Head/Neck Model to 10 $G_z$<br>Acceleration.....  | 75 |
| 6.2  | Comparison of Z-direction Head Acceleration During<br>10 $G_z$ Ejection from Experimental Data and Original<br>ATB Model Simulation.....     | 76 |
| 6.3  | Response of Modified ATB Head/Neck Model to 10 $G_z$<br>Acceleration.....  | 78 |
| 6.4  | Comparison of Z-direction Head Acceleration During<br>10 $G_z$ Ejection from Experimental Data and Modified<br>ATB Model Simulation.....     | 79 |
| 6.5  | Response of Viscoelastic ATB Head/Neck Model to<br>10 $G_z$ Acceleration.....  | 81 |
| 6.6  | Comparison of Z-direction Head Acceleration During<br>10 $G_z$ Ejection from Experimental Data and<br>Viscoelastic ATB Model Simulation..... | 82 |

# List of Symbols

| <u>Symbol</u>    | <u>Definition</u>   |
|------------------|---|
| $m$              | the mass of the segment   |
| $\vec{x}$        | the acceleration of the segment center of mass<br>(in inertial reference frame)   |
| $\vec{F}$        | the sum of all external forces applied to the<br>segment  |
| $\vec{H}$        | the rate-of-change of angular momentum of the<br>segment about its center of mass   |
| $\vec{N}$        | the sum of all moments about the body center<br>of mass from all forces applied to the body<br>plus the sum of all force couples (torques)<br>applied to the body |
| $M$              | the mass matrix   |
| $A_{ij}, B_{ij}$ | system matrices calculated from known system<br>physical input  |
| $\Phi$           | the inertia matrix  |
| $\ddot{X}$       | the translational acceleration matrix   |
| $\dot{\omega}$   | the angular acceleration matrix   |
| $f$              | the joint constraint force matrix   |
| $t$              | the joint constraint torque   |
| $q$              | the special constraint force matrix   |

|                 |   |
|-----------------|---|
| $\tau$          | the flexible element constraint torque matrix   |
| $U_1$           | the external force  |
| $U_2$           | the external torque   |
| $V_j$           | the constraint forcing function matrix  |
| $\bar{X}_n$     | the position of the segment n center<br>of gravity in the inertial reference frame  |
| $D_n^{-1}$      | the inverse direction cosine matrices which<br>transform from the inertial coordinate system<br>to the local coordinate system                    |
| $\bar{I}_{nj}$  | position of joint j in the local reference frame  |
| $T_{TOTAL}$     | the total torsional resistance (in-lbs) of the<br>joint to rotation   |
| $T$             | the joint torque (in-lbs) due to muscles and<br>ligaments   |
| $T_s$           | the joint torque (in-lbs) due to the anatomical<br>joint limit  |
| $\theta$        | the relative angular displacement (deg) between<br>joint Z-axes of the two joined segments,   |
| $S_1, S_2, S_3$ | the linear, quadratic, and cubic torque<br>coefficients (in-lbs/deg), (in-lbs/deg <sup>2</sup> ), and<br>(in-lbs/deg <sup>3</sup> ), respectively |
| $S_4$           | the energy dissipation coefficient (a<br>dimensionless variable between 0 and 1)  |
| $S_5$           | the limiting joint stop angle (deg) with  |

|                    |  |
|--------------------|--|
|                    | respect to the center of symmetry  |
| $T$                | the resistance (in-lb) to rotation due to rate $\dot{\theta}$ relative segment rotation,       |
| $ \omega $         | the magnitude of the relative angular velocity (deg/sec) between two jointed segments          |
| $V_1$              | the linear viscous coefficient (in-lb-sec/deg)   |
| $V_2$              | the coulomb friction coefficient (in-lb)   |
| $V_3$              | the relative angular velocity (deg/sec) of the joint at which full coulomb friction is applied |
| $\max(a, b)$       | the greater value: a or b  |
| $I_N$              | the segment principle moments of inertia   |
| $\vec{d}$          | the amount of slip joint displacement (in)   |
| $\vec{F}_{spring}$ | force (lb) applied to joined segments by the slip joint spring                                 |
| $\vec{F}_{damper}$ | force (lb) applied to joined segments by the slip joint damper                                 |
| $k_1, k_2$         | linear (lb/in) and quadratic (lb/in <sup>2</sup> ) slip joint spring coefficients              |
| $c$                | slip joint viscous damping coefficient (lb-sec/in)   |

# 1.0 Introduction

U.S. Navy ejection statistics (1) show that 1,677 emergency aircraft ejections were accomplished clear of the aircraft and within the escape systems terrain clearance envelope between the years 1968 and 1988. However, 1.67% of the ejectees were reported to have sustained cervical fractures and 12.16% paracervical sprains and strains. An analysis of the above ejections led researchers to suggest caution be exercised in "the current trend to integrate manifold system's elements into aircrew helmets" due to the potentially dangerous added mass to the head or altered head center of gravity. While improving the aviators' ability to operate effectively, the addition of Helmet Mounted Displays (HMD) and Night Vision Goggles (NVG) to jet pilot helmets may also increase the risk of pilot neck injury in the flight, impact, and ejection environments (1,2).

In order to quantify the increased potential for injury during ejection, the United States Air Force is currently conducting a program to evaluate the response of the human head and neck to various  $G_z$  accelerations (Figure 1.1) when head mass and mass distribution are altered by the addition of NVG/helmet combinations (3). The program, conducted at the

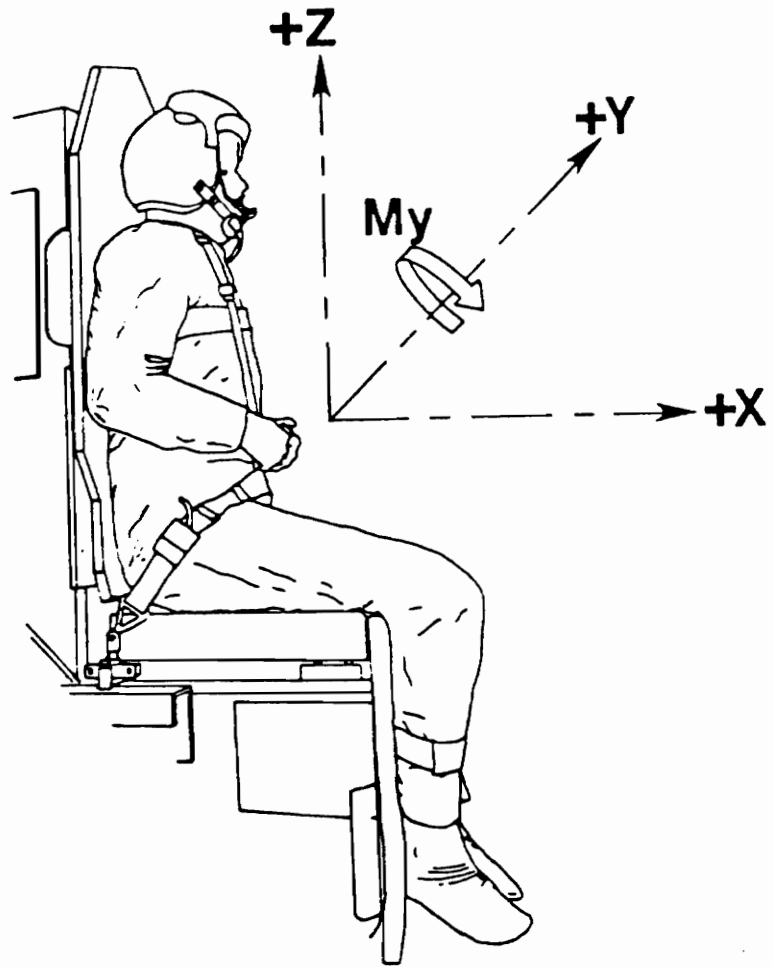


Figure 1.1 Test Configuration for Seated Human Subject  
with Added NVG/Helmet Combination

Armstrong Laboratory located at the Wright-Patterson Air Force Base, Ohio, includes vertical impact testing with manikins and volunteers and computer modeling analysis of the head/neck system dynamic response to  $G_z$  accelerations. The goal of the program is to develop limiting design criteria for future helmet/helmet-mounted systems and to evaluate current prototypes based on this criteria.

Computer simulations are valuable for predicting the human biodynamic response to adverse environments that are unsafe for human testing; and for providing stress/strain and/or stress/strain-rate information impossible to measure directly in the live human subjects. Computer simulations are a desirable alternative to anthropometric manikin testing because of shortcomings in the ability of the manikins to mimic live human response and the high cost of full scale manikin testing. The kinematic and dynamic response data obtained from computer simulations can be used to define a response mechanism and to analyze the forces sustained within the structure of the system. The first step in producing a model of the human system is to develop an analog of the system and to validate it with known human response information. The subject of the work described herein will be the validation of a proposed viscoelastic model of the human head/neck system against experimental data.



The Articulated Total Body (ATB) model was used in the development of computer simulations of the human head and neck. The Articulated Total Body model is a computer simulation program which uses three-dimensional rigid body dynamics to predict gross human body response to various dynamic environments (4). The original program was the Crash Victim Simulation (CVS) program developed for the Department of Transportation by the Calspan Corporation to study the three-dimensional contact force environment and dynamics of a motor vehicle crash victim (5). Aerodynamic force application and harness belt capability were added in 1975 by Calspan for the Armstrong Laboratory, thereby creating the first version of the ATB. The program was modified throughout the 1980's to produce the current ATB-IV version which includes the capability to simulate aircraft ejection with windblast exposure as well as complex automobile accidents (4).

The living human responds both passively and actively to changes in its environment. The head/neck system used in the ATB program can simulate the effects of joint motion limitations, friction in the joints, ligament forces and active reflex muscle contraction. However, the current model neck characteristic fails to properly represent the passive viscoelastic axial deformation properties of the cervical spine. Human tests indicate significant compression and bending of the neck during ejection accelerations. It is the

intent of this thesis to improve upon the current head/neck characterization used in the ATB model. In particular, the work described herein will propose and validate a characterization for the ATB model based on nonlinear viscoelastic properties of the cervical spine.

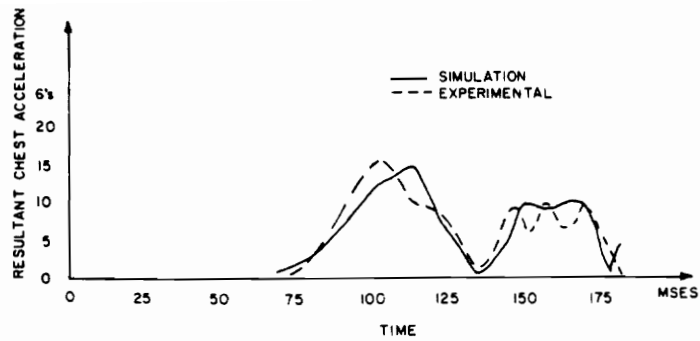
## 2.0 Literature Review

The potential for, and identification of mechanisms of human injury have grown with the evolution of automotive and aircraft technology. To facilitate the quantification, prediction and simulation of human biodynamic response to dynamic environments with a minimum of human and/or animal experimentation, many computerized mathematical models of human body structure have been developed. These models include internal body structure models and external gross motion body models (6). Internal body structure models are used to predict stresses, strains, and localized displacements of a body subsystem such as the neck or the spine. External gross motion body models are used to predict whole body motion and body segment interactions.

The ATB model has been developed at the Armstrong Laboratory for predicting gross human body responses to various dynamic environments (3). Kaleps (6) used a 15 segment/14 joint representation of the human body with the ATB model to predict human response to whole body  $-G_x$  impact. The type of joints used were ball-and-socket except for the knees and elbows where pin joints were used. The effect of a harness restraint was included in the model.

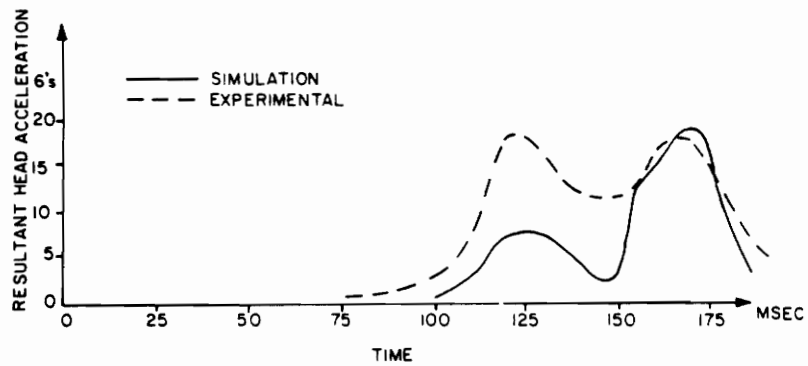
The results were compared to experimentally observed human responses to 6, 8, and 10 G dynamic exposures, and most of the calculated body segment accelerations were predictive of experimentally observed accelerations, such as the resultant chest acceleration shown in Figure 2.1A. However, comparisons of simulated and measured head accelerations showed the amplitude of the head segment resultant acceleration of 10 G's to be only about half of the 20 G's observed in experiment (Figure 2.1B). The model was not suited for detailed analysis of the complex articulated motion of the cervical spine, the multiple articulations of which were modeled by two ball-and-socket joints at both the head/neck and the neck/torso junctions. The model was not capable of accounting for pre-tensing of the neck muscles (subject anticipation of impact), or voluntary actions of the muscles during the impact event. These effects were observed to be a significant factor in head/neck response to low G level acceleration (6 to 10 G's).

Efforts to improve the ability of this model to simulate head/neck system response to acceleration were made by Frisch and Cooper (7). Simulations of the head and neck system response to  $-G_x$  acceleration were performed using a measured deceleration profile (X- and Z-directions) at the first thoracic vertebra, T1, as the driving function of the



2.1A

Comparison of simulated and experimental resultant chest acceleration during 10-g peak  $-G_x$  impact.



2.1B

Comparison of simulated and experimental resultant head acceleration during 10-g peak  $-G_x$  impact.

Figure 2.1 A) Comparison of Kaleps' Simulated and Experimental Resultant Chest Acceleration During 10 G Peak  $-G_x$  Impact. B) Comparison of Kaleps' Simulated and Experimental Resultant Head Acceleration during 10 G peak  $-G_x$  impact.

head/neck system. The neck in this model was represented by a rigid segment pivoting at T1 with respect to the thorax and at the first cervical vertebra, C1, with respect to the head. An alternate head pivot location based on analysis of head rotation shown on high speed films was also used for comparison.

Both joints were modeled as ball-and-socket joints restricted by friction and viscous retarding forces. Joint limiting angles were applied to the two joints such that relative rotation between the joined segments beyond the joint limiting angle would be opposed by quadratic and cubic springs to restore the segment excursion back to within its joint stop contour. The head ranges of motion were initially set for 22.5 degrees flexion and 18.9 degrees extension (forward and backward rotation, respectively) for the head relative to the neck, and 61.9 degrees flexion and 61.5 degrees extension for the neck relative to the T1 platform. The initial estimates of the forcing elements were obtained from Becker's (8) preliminary analysis of the subject data illustrated in Figure 2.2. The head/neck forcing element possessed a spring coefficient of 62 in-lb/deg for angles above 5 degrees and damping coefficients of 0.1 in-lb-sec/deg for loading and 0.41 for unloading of the joint. The neck/torso possessed a spring coefficient of 15.5 in-lb/deg for angles below 79 degrees and

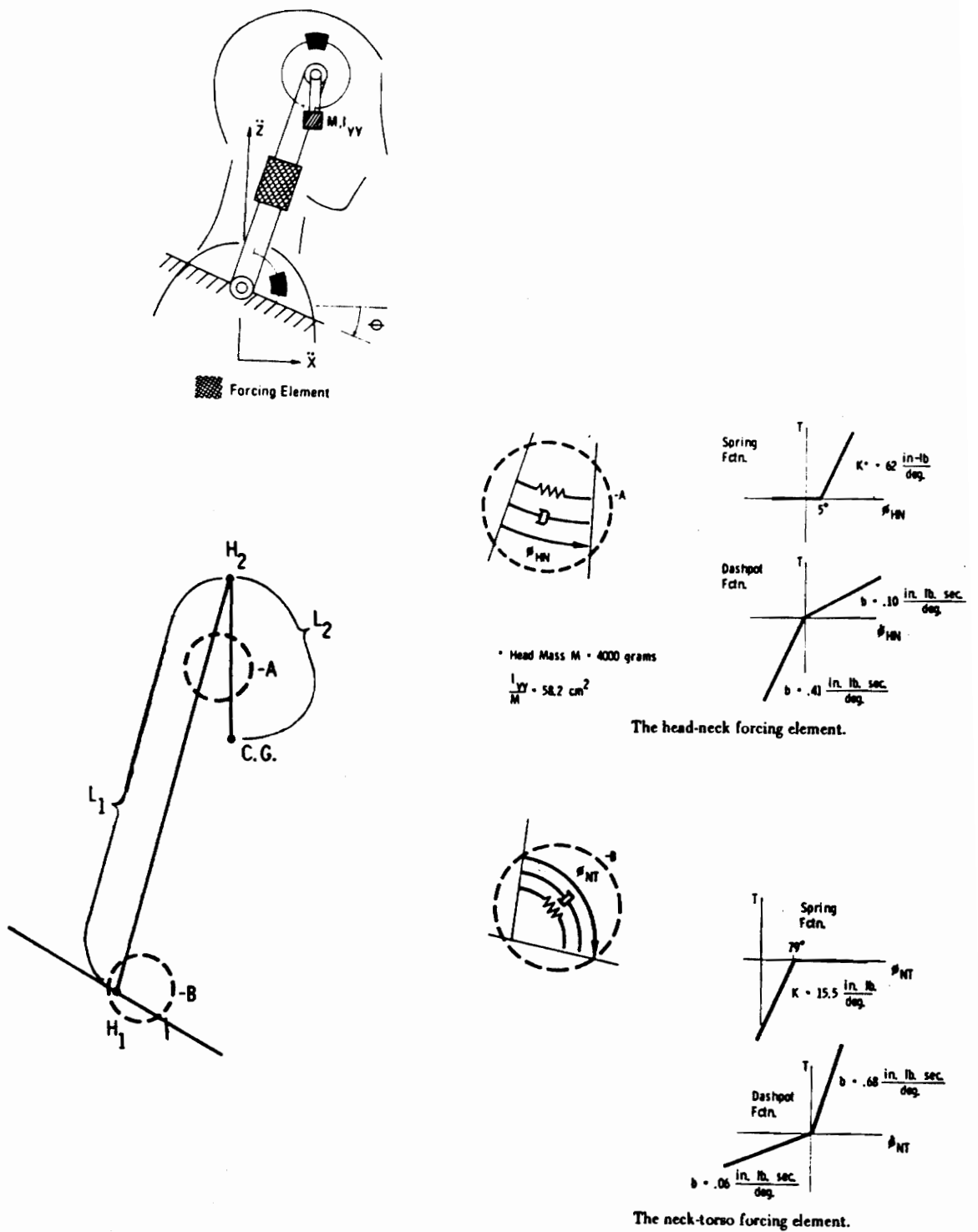


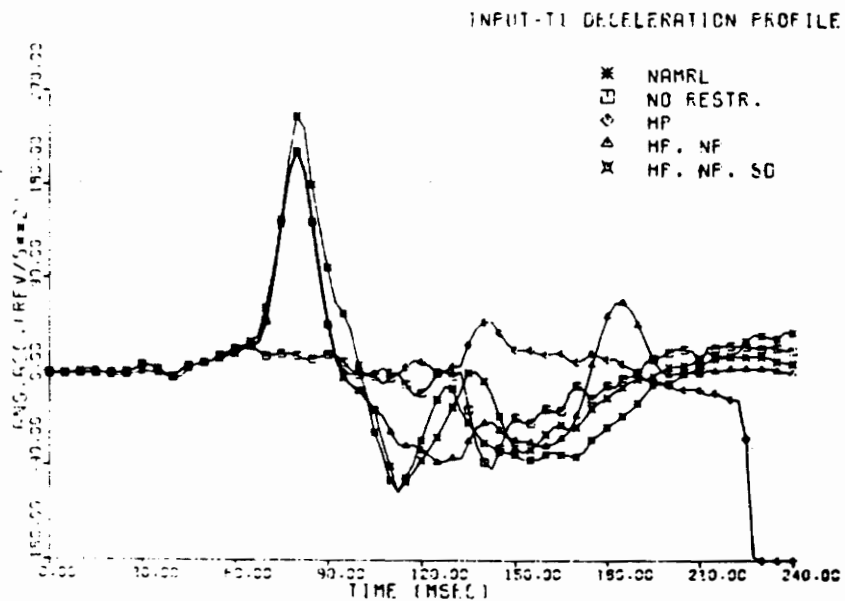
Figure 2.2 Becker's Head/Neck System Joint Forcing Elements

damping coefficients of 0.68 in-lb-sec/deg for loading and 0.06 for unloading (8).

The angle and stiffness of the head/neck joint stop were adjusted based on an analysis of the angular relationship existing between the head and the neck. The neck angle was defined as the angle that the neck vector (a vector from T1 to the head pivot location) made with the Z-axis of the inertial reference frame. The head to neck angle was defined as the angle the neck vector made with the head anatomical coordinate system. The average estimated joint limiting angles were 22.61, 22.54, and 35.12 degrees for 8, 9, and 15 G simulations, respectively, at an average of 66, 65 and 78 ms.

As a result of discrepancies between computer simulation and experimental human test data, it was proposed by Frisch and Cooper that ligament effects must also contribute to the biodynamic response of this anatomical region. To simulate the ligament restrictions, such as from the ligamentum nuchae, a parallel spring and damper was introduced into the model. The attachment points of the spring and damper were at the base of the skull and at T1. The results shown in Figure 2.3 show improvement in the simulated head angular acceleration compared to the Naval Aerospace Medical Research Laboratory (NAMRL) test data when the three elements described above were added to the characteristic.





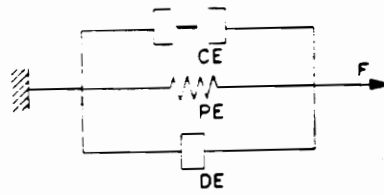
Head angular acceleration with head pivot at HP<sub>2</sub> and varying restrictions to head-to-neck articulation. NO RESTR.= no head or neck pivot. HP=only head pivot included. HP,NP= head pivot and neck pivot included. HP,NP,SD=head pivot, neck pivot and spring-damper included.

Figure 2.3 Comparison of Frisch and Cooper's Simulated and NAMRL Experimental Head Angular Acceleration During a 9.8 G Peak  $-G_x$  Impact

To further improve the ATB model's representation of human biodynamic response to acceleration, including voluntary and reflex responses, Freivalds and Kaleps (9) incorporated active neuromusculature into the ATB model. The simplified muscle model was composed of three elements: a contractile element (CE), parallel damping element (DE), and parallel elastic element (PE), each representing a different property of human muscle. The strength of the muscle was calculated from the forcing functions of muscle strain and strain rate in Figure 2.4. Four major muscle groups were modeled. The interior and exterior obliques; and the psoas, erector spinae, and quadratus lumborum were modeled for the trunk. The trapezius; and the scalenus, levator scapulae, and sternocleidomastoid were modeled for the neck.

Computer simulations were prepared for the response of a male air crew member to a number of  $G_y$  lateral impacts. The results were then compared to simulations of human response to identical conditions without the added musculature. At the end of 256 ms, the angular displacement of the upper trunk was reduced by 12 degrees with the use of musculature. However, no validation of the results by comparison with experimentally measured human response was attempted.

The human body model developed by Freivalds and Kaleps, including the active muscle addition, was used by Freivalds



Simplified muscle model.

$$f(\epsilon, \dot{\epsilon}) = F_1(\epsilon) + F_2(\epsilon) \cdot F_3(\dot{\epsilon}) + F_4(\dot{\epsilon})$$

$$F_1(\epsilon) = 0.00163(e^{2.66\epsilon} - 1)F_{MAX}$$

$$F_2(\epsilon) = 0.32 + 0.71 e^{-1.112\epsilon} \sin(3.722(\epsilon + 0.344))$$

$$F_3(\dot{\epsilon}) = 0.1433\{0.1074 + e^{-1.409 \sinh(1.1\dot{\epsilon} + 1.6)}\}^{-1}F_{MAX}$$

$$F_4(\dot{\epsilon}) = 0.32\dot{\epsilon} \cdot F_{MAX}$$

where  $\epsilon = (l - l_0)/l_0$  and  $l$  is the instantaneous and  $l_0$  the resting muscle length and  $F_{MAX}$  is the maximum isometric tension of the muscle.

Figure 2.4 Forcing Functions for Freivalds and Kaleps' Muscle Model

and McCauley (10) in a study to evaluate the effects of helmet mass and center of gravity on biodynamic response to an ejection environment. The 15 segment/14 joint model was used with male anthropometry and segment, joint, and muscle properties from Freivalds and Kaleps (9). The simulation was created with the human body model in a seated posture based on the design specifications of the AV-8B aircraft ejection seat, and a driving acceleration profile based on the ejection profile characteristics of the AV-8B. The effects of weight, location of the head center of gravity, and the initial resting angle of the head and neck were investigated. Three weights were chosen, 0, 1.36 and 2.73 kg, to represent various helmets. Three locations of assembly center of gravity were chosen: 0, 2.54, and 5.08 cm offset. Three angles for initial head/neck position were used: -15, 0, and 15 degrees. The authors concluded from the results of the simulations that additional mass had little effect on head injury, while a combination of cg-offset and initial head-rest positions could result in significant head rotation, head torque and head-injury scale values.

The validation of the ATB human body model for  $G_z$  accelerations has not been documented, since volunteer  $G_z$  impact data on neck response has only recently become

available (18). It is the focus of this work to evaluate the fidelity of ATB model response simulations for  $G_z$  impacts.

## 3.0 Operational Background

### 3.1 General Formulation of the ATB Model

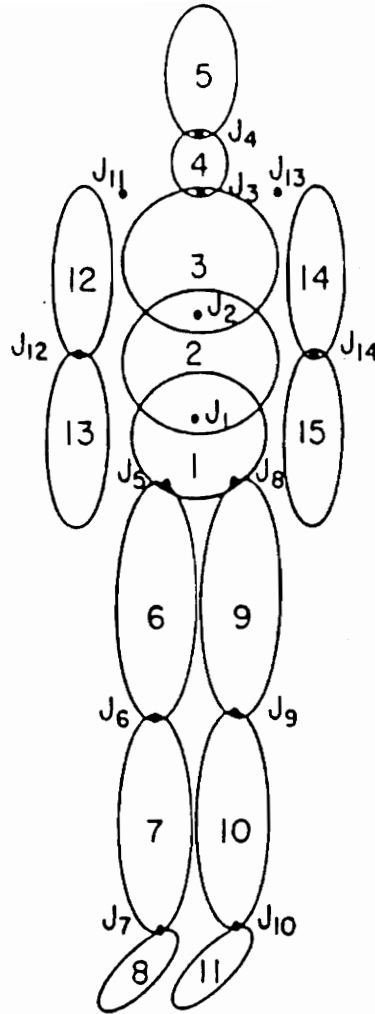
The ATB Model is a computer program that predictively calculates the three-dimensional dynamic response of a system of articulated rigid bodies subjected to a dynamic environment of externally applied forces and interactive contact forces (4). The system to be simulated contains one or more rigid segments which can be connected in an open chain structure (containing no closed loops of connected segments) or the segments can be free (i.e. not connected), representing physical surroundings. The maximum number of segments allowed by the ATB model is 30.

By modeling the human body as a system of connected rigid segments, the ATB model can be used to predict the dynamic response of the human body to various environments. The standard 15 segment/14 joint model of the human body used in car crash and aircraft ejection simulations (4) is shown in Figure 3.1 with segments representing the lower torso, center torso, upper torso, neck, head, upper arms, lower arms, upper legs, lower legs, and feet. The body segments and joints are assigned identification numbers: from one to NSEG for the

segments, where NSEG is the total number of segments (e.g. 15), and from one to NJNT for the joints, where NJNT is the total number of joints (e.g. 14) connecting the segments. The contact surface of each segment is defined by a corresponding ellipsoid illustrated in Figure 3.1.

Six primary coordinate systems are defined in the ATB model to facilitate describing the input parameters for the simulation and to provide sufficient reference systems for convenient analysis of output information. These coordinate systems include: local body segment, principal, joint, contact ellipsoid, inertial, and vehicular. The inertial, local, and joint coordinate systems are the most pertinent to the current study and are defined here.

The location of the inertial reference frame origin may be placed at any convenient point in space and the locations of all other coordinate systems are specified with respect to this point. Although the orientation of the inertial frame of reference is optional, provided it is a right handed system, one which defines the positive Z-axis to be in the direction of the gravity vector toward the center of the earth is advised. The inertial reference frame then remains fixed in space regardless of the orientation of the subject. Thus, as shown in Figure 3.2, the inertial coordinate system of the head and neck, when using the ATB model for impact and aircraft ejection simulations, is defined such that: the



Joint  $j$  connects segment  $JNT(j)$  with segment  $j+1$ .

Figure 3.1 Standard ATB 15 Segment/14 Joint Model of the Human Body



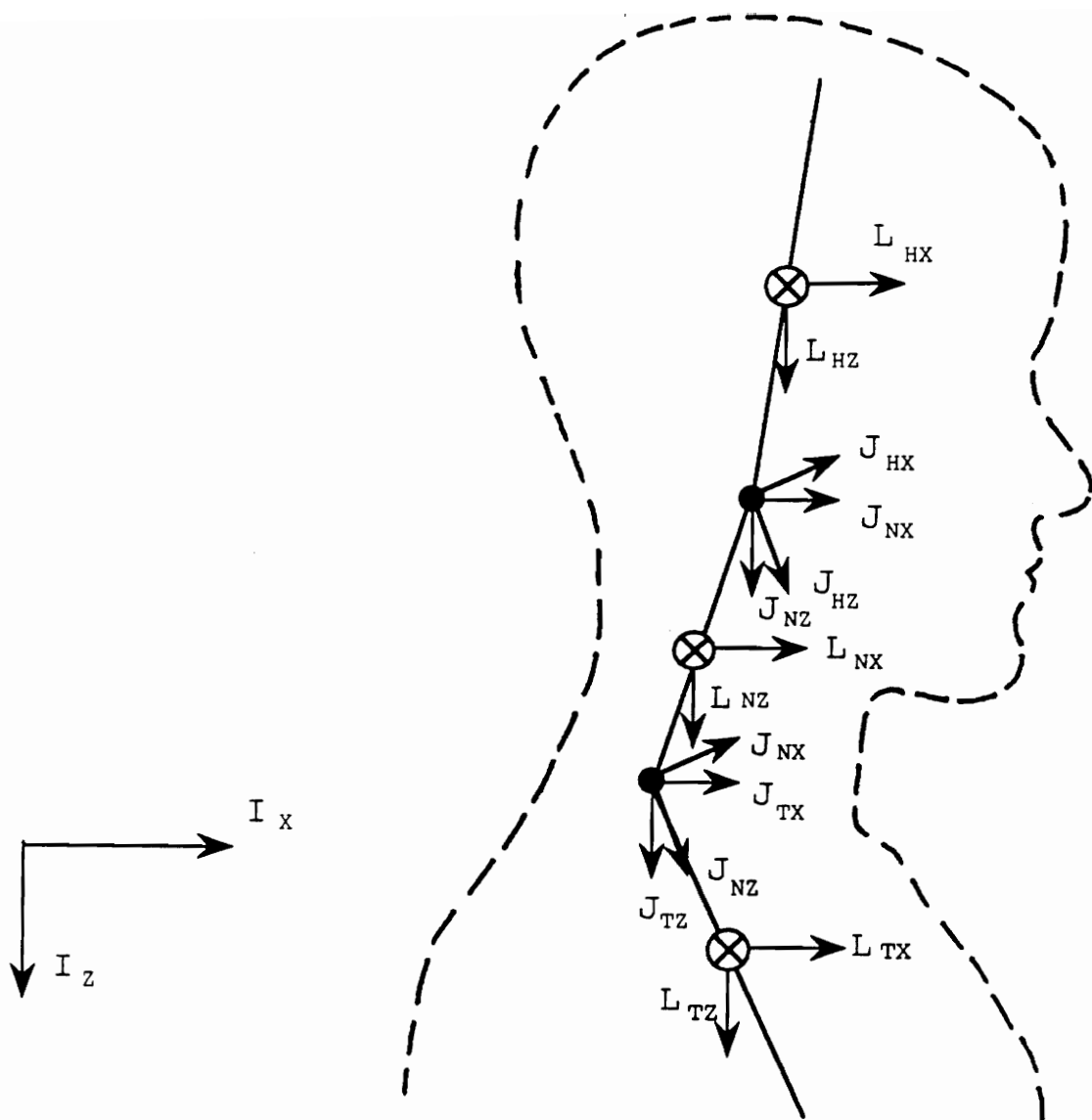


Figure 3.2 Inertial, Local, and Joint Coordinate System of the ATB Head/Neck Model

direction from the back of the upright seated subject towards the chest is the direction of the positive X-axis, the direction from the head of the upright seated subject towards buttocks is the direction of the positive Z-axis, and the lateral direction from the left side of the subject towards the right side is the direction of the positive Y-axis. It is noted that the ATB coordinate system is rotated 180 degrees about the X-axis of the laboratory coordinate system used in measuring human test data (the positive Y- and Z-axes are in opposite directions).

Each body segment has a local reference coordinate system (Figure 3.2). The origin of this system is at the segment center of mass. Although the orientation of the local coordinate system is also optional, one consistent with the inertial system is advised. Physical characteristics of the body such as the dimensions of the contact ellipsoids, the orientation of the principal axes of inertia with respect to the local segment coordinate system, and the location of the joint(s), are defined with respect to the local reference frames.

Two coordinate systems are defined at each joint (Figure 3.2), one rigidly attached to each of the respective segments connected at that joint. The origin of the coordinate systems respectively coincide with the corresponding anatomical location of the joint, and the coordinate axes for each joint

coordinate system are described with respect to the local coordinate system of the segment to which it is attached. Torques are applied at the joint locations in order to simulate the resistance to rotation contributed by the surrounding tissue. These joint torques are computed as functions of the relative orientation of the two joint coordinate systems.

The input to the ATB program is divided into eight categories referred to as cards (4,5):

- Cards A    Date and run description, units of input and output, control of restraint integrator, and optional output;
- Cards B    Physical characteristics of the segments and joints including: the number of segments and joints, the segment weights and inertias, the joint locations, and the resistive torque coefficients;
- Cards C    Description of the vehicle motion in terms of position, velocity, or deceleration;
- Cards D    Contact planes, belts, air bags, contact ellipsoids, constraints, and symmetry options;
- Cards E    User defined functions defining force deflections, inertial spike, energy absorption factor, and friction coefficients;

Cards F    Allowed contacts among segments, planes, belts, air bags, and contact ellipsoids;  
Cards G    Initial orientations and velocities of the segments;  
Cards H    Control of the time history output of selected segment motions and joint parameters.

The format requirements, the required input frames of reference, and detailed card descriptions are given in Reference 4.

### 3.2 System Equations

The system equations were derived by considering each segment to be a free rigid body subjected to the forces and torques of constraint and of external contacts (5). The general motion of a rigid body includes rotation plus translation. Thus, the corresponding equations of motion (11) are:

$$\sum \vec{F} = m\ddot{\vec{x}} \quad [3-1]$$

and

$$\sum \vec{N} = \dot{\vec{H}} \quad [3-2]$$

where

|                  |   |
|------------------|---|
| $m$              | = the mass of the segment,  |
| $\ddot{\vec{x}}$ | = the acceleration of the segment center of mass<br>(in inertial reference frame),  |
| $\Sigma \vec{F}$ | = the sum of all external forces applied to the<br>segment,   |
| $\dot{\vec{H}}$  | = the rate-of-change of angular momentum of the<br>segment about its center of mass,  |
| $\Sigma \vec{N}$ | = the sum of all moments about the body center<br>of mass from all forces applied to the body,<br>plus the sum of all force couples (torques)<br>applied to the body. |

The effect of joint constraints is applied in a method unique to the ATB model. It is similar to the Newtonian method in that constraint forces are explicitly contained in the equations of motion. However, the ATB model uses constraint relations of the type employed in the Lagrange method, i.e. functions of position and velocity, rather than force constraints, which are then differentiated to functions of acceleration in the system equations. The details of this method are defined, and an equivalence analysis is performed in Reference 11.

The dynamic equations for each segment are combined into a matrix equation where the variables for each segment become elements in matrix variables for the entire system. The

resulting system matrices used in the ATB model for a system of rigid bodies are described in matrix form below:

$$\begin{bmatrix} M & 0 & A_{11} & 0 & A_{13} & 0 \\ 0 & \Phi & A_{21} & A_{22} & A_{23} & A_{24} \\ B_{11} & B_{12} & B_{13} & 0 & 0 & 0 \\ 0 & B_{22} & 0 & B_{24} & 0 & 0 \\ B_{31} & B_{32} & 0 & 0 & B_{35} & 0 \\ 0 & B_{42} & 0 & 0 & 0 & 0 \end{bmatrix} \begin{bmatrix} \ddot{X} \\ \dot{\omega} \\ f \\ t \\ q \\ \tau \end{bmatrix} = \begin{bmatrix} U_1 \\ U_2 \\ V_1 \\ V_2 \\ V_3 \\ V_4 \end{bmatrix} \quad [3-3]$$

where

- $M$  = the mass matrix,
- $A_{ij}, B_{ij}$  = system matrices calculated from known system physical input, where  $i$  and  $j$  are as indicated above,
- $\Phi$  = the inertia matrix,
- $\ddot{X}$  = the translational acceleration matrix,
- $\dot{\omega}$  = the angular acceleration matrix,
- $f$  = the joint constraint force matrix,
- $t$  = the joint constraint torque matrix,
- $q$  = the special constraint force matrix,
- $\tau$  = the flexible element constraint torque matrix,
- $U_1$  = the external force matrix,
- $U_2$  = the external torque matrix,
- $V_j$  = the constraint forcing function matrix.

The first equation of matrix [3-3] is the linear equation of motion derived from Newton's equation [3-1] above. External forces are incorporated into the system equations here, including those from the linear spring and damper systems applied to the segments (functions of linear displacement/rate of linear displacement), i.e. the spring and damper system applied at the neck/torso joint in Chapter 5.3. The second equation of the matrix is the angular equation of motion derived from Euler's equation [3-2] above. External torques are incorporated into the system equations here, including those from the torsional spring and damper systems applied to the joints, i.e. the torsional spring and damper systems applied to the head/neck and neck torso joints in Chapter 4.2. A constraint force matrix  $q$  was introduced into both equations of motion, to be determined by the four subsequent constraint equations in the matrix.

The third equation of the system matrix [3-3] is the linear constraint equation which is derived from the linear position constraint stated here for two joined segments  $m$  and  $n$ :

$$\vec{X}_n + D_n^{-1} \vec{I}_{nj} = \vec{X}_m + D_m^{-1} \vec{I}_{mj} \quad [3-4]$$

where

$\vec{X}_n, \vec{X}_m$  = the position of the respective segment centers of gravity in inertial reference frames,

$D_n^{-1}, D_m^{-1}$  = the inverse direction cosine matrices which transform from the inertial coordinate system to the local coordinate system, and  
 $\vec{r}_{nj}, \vec{r}_{mj}$  = position of joint j in the respective local reference frames.

This constraint ensures that the segments do not separate at the joint location so the joint location approached from either segment will define the same point in space. This constraint must be enforced for Euler, pin, and ball-and-socket joints. However, this constraint is modified for a slip joint as described in Chapter 5.3.

The fourth system equation of [3-3] is the angular constraint equation derived from the joint rotational constraint. This constraint is dependent on the type of joint at the articulation. For example, a pin joint will have rotational freedom about the local Y-axis but will be constrained from rotational motion about the local X- and Z-axes.

The fifth system equation of [3-3] is a type of distance constraint to account for rolling and sliding of segments against each other and against the physical surroundings. The final constraint equation in the matrix is derived for the flexible element option incorporated into the ATB model, which



allows a single segment in the system to be composed of several smaller segments.

## 4.0 Problem Statement and Formulation

### 4.1 Anatomical Description of the Human Head and Neck

The human head encompasses the brain, sense organs, including the eyes, ears, nose and mouth, and 29 bones which form the skull. There is, however, only one movable joint in the head: the temporomandibular joint of the jaw. Thus, the gross dynamic motion of the human head may be considered (as a first approximation) to be that of a single entity, a rigid mass. In contrast, the human neck consists of seven cervical vertebrae with a joint at the articulation of the neck with the head, one at the articulation of the neck with the thoracic spine, and one between each vertebral articulation. Each neck joint allows restricted motion of the articulated segments, contributing individually to the collective dynamic motion of the human neck.

The seven cervical vertebrae which make up the skeletal portion of the neck (C1-C7 numbered top to bottom) are illustrated in Figure 4.1. The first two vertebrae are unique in shape and are labeled the atlas (C1) and the axis (C2). The remaining vertebrae are characterized by four segments (12):

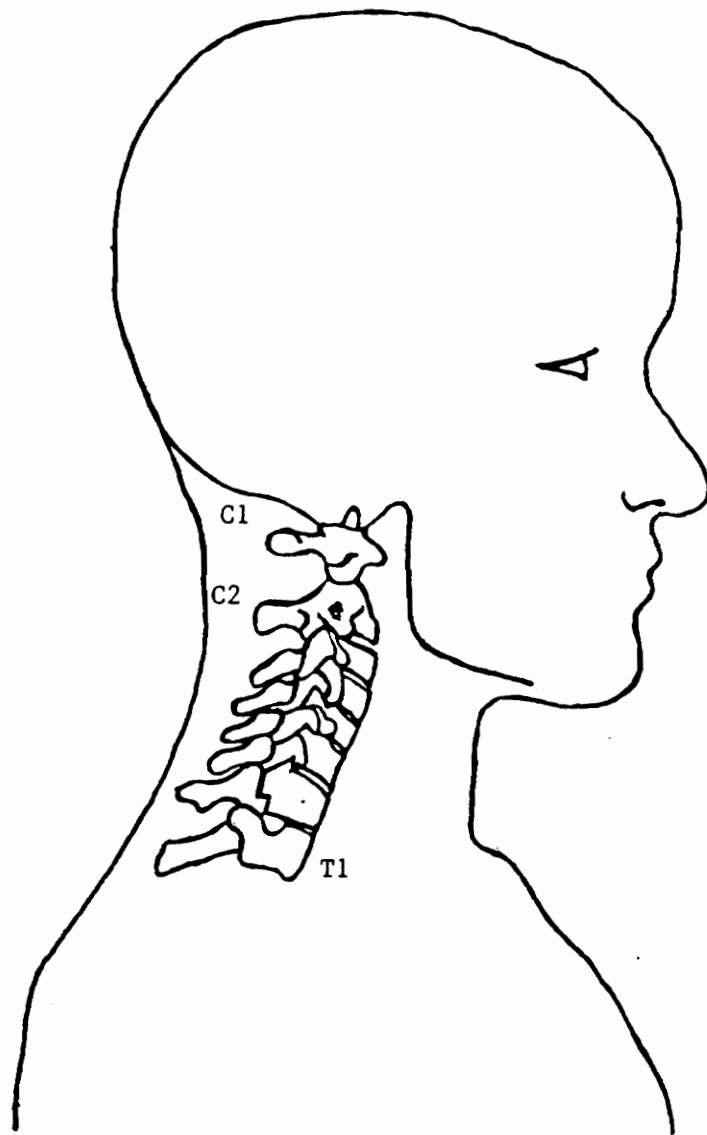


Figure 4.1 Anatomical Representation of the Human  
Head/Neck System

- 1) The vertebral body, which is a thick, oblong portion of bone on the ventral (stomach) side of the spinal column;
- 2) The vertebral arch, which projects ring-like from the back of the vertebral body, enclosing a passage (the vertebral foramen) for the spinal chord, and which is equipped with three projections for muscle and ligament attachment: one transverse process on each side at the origin of the arch from the vertebral body, and one spinous process in the back at the middle or "top" of the arch;
- 3) The four articular processes, which are smooth surfaces on the lateral masses of the vertebrae for the articulation of adjacent vertebrae; and,
- 4) The intervertebral foramen, which are canals in the articulated column allowing for the passage of peripheral nerves to (sensory, or afferent) and from (motor, or efferent) the spinal chord.

The atlas is a ring shaped bone with no body. Two processes on the occipital bone at the base of the skull, called the occipital condyles, rest on the top (superior) articular processes of the atlas forming the Atlanto-Occipital joint (12). This joint permits the motions involved in the forward (flexion) and backward (extension) nodding (as if to say "Yes") of the head (13,14) as shown in Figure 4.2. There is also slight lateral bending permitted

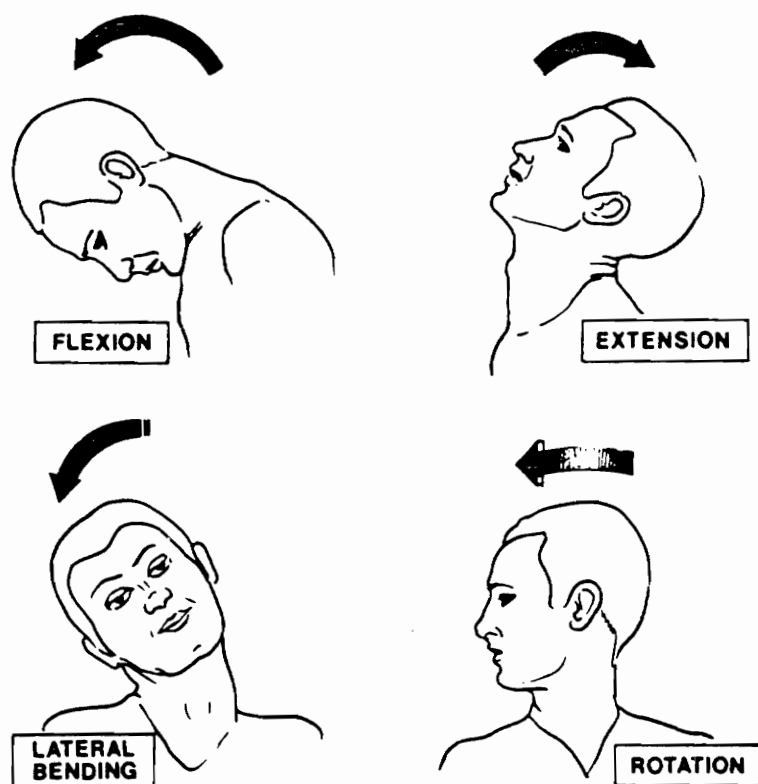


Figure 4.2 Motions Involved in Head Movement (21)

at this articulation, which is involved in ear to shoulder rotation.

The articulation of the atlas and the axis forms the central atlanto-axial joint (12). The shape of the axis is similar to the characteristic vertebrae described above with an added tooth-like process (the odontoid process) projecting from the top of the body. The atlas fits over and rotates about this process. The resulting joint allows rotation of the head left or right (as if to say "No") about an axis formed by the odontoid process (Figure 4.2).

Each subsequent pair of cervical vertebrae allows relative rotational and sliding motion at the respective articulation and cumulatively contributes to head and neck motion. The amount of motion allowed at each vertebral joint is limited by passive constraints. Between each of the vertebrae is a fibrocartilaginous disc which is inseparable from the bodies of the adjacent vertebrae. This disc allows limited movement between the vertebrae while also acting as a shock absorbing mechanism. A complex connecting structure composed of fibrous bands called ligaments also limits the range of movement between vertebrae. Vertebrae of the cervical spinal column are attached by longitudinal ligaments which extend the length of the spine and by smaller ligaments which attach only adjacent parts of two vertebrae. Capsular ligaments attach articular processes of adjacent vertebrae

enclosing a structure characteristic of a moveable joint. Synovial fluid and articular cartilage exist at this intervertebral location which allows much of the neck movement.

Active motion of the head and neck is controlled by several of the muscles in the head, neck and upper back regions of the body (12). Head motion is controlled by the sternocleidomastoid, the trapezius and the splenius capitis muscles. The sternocleidomastoid muscle is a large thick muscle which passes along the side of the neck. It originates from the sternum (chest bone) and clavicle (collar bone) of the upper chest and inserts at the temporal and occipital bones to the skull below and behind the ear. When this muscle contracts on one side, the head is rotated to the opposite side. When it contracts on both sides, the head is drawn down and forward.

The splenius capitis is a broad, flat muscle that originates at the top three thoracic and the seventh cervical vertebrae and also inserts at the temporal and occipital bones of the skull. This muscle contributes to the extension of the head if both sides contract or the turning of the head to the side if only one side contracts.

The trapezius muscle is a broad flat triangular muscle that covers the neck, upper back and shoulders. It originates at points along the center of the back, including

the occipital bone, the ligamentum nuchae, and the spinous processes, spreads out onto the shoulders, and inserts at the chest at the scapula and the clavicle. When the head is fixed, it moves the shoulders and when the shoulders are fixed, it moves the head. The head is extended when both sides contract or turned to the opposite side when one side contracts.

Longer thinner groups of muscles support the vertebral column as well as move the head. Longissimus and spinalis muscles of the erector spinae originate from the thoracic transverse and spinous processes respectively. The longissimus muscles insert at the transverse processes of the cervical vertebrae and the temporal bone. The spinalis muscles insert at the spinous process of the axis and the occipital bone. These muscles extend the vertebral column and bend it laterally or contribute to the head motion controlled by the splenius capitis. Also controlling the cervical spine are small intervertebral muscles, such as the intertransversalis which are placed between pairs of transverse processes.

Movements of the head and spine are determined by the type of joints between the skeletal segments, the stretch of the ligaments along the neck, and muscles along the cranium, neck, and upper back. This motion is presented qualitatively in the literature (12,13,14) in the manner of the head/neck



description presented above. The mechanical properties of the discs, ligaments, and muscles are not quantitatively documented due to the state and environment dependent nature of live biological tissue. Muscle, for example, exhibits time-dependent, nonlinear viscoelastic behavior (15). The viscoelastic properties are inconsistent when measured in vivo (in a living human) and in situ (in an intact physiological environment outside of the human body). Muscle requires at least 10 ms to begin contracting from the time the signal is sent from the brain (15). Thus, head/neck response to impact acceleration includes both passive and active muscle response. Viscoelastic properties of muscle have also been shown to be sensitive to electric excitation (16) indicating that the mechanical properties of active muscle differ from those of inactive or passive muscle.

#### **4.2 Computer Model of the Head and Neck**

The idealization currently used in the ATB model to describe the human head/neck system consists of three rigid segments connected by two ball-and-socket joints (Figure 4.3). The three segments represent the skull, the cervical column and the upper torso. The ball-and-socket joints allow for relative rotational motions between these body segments. The extension-flexion motion of the head allowed by the atlanto-

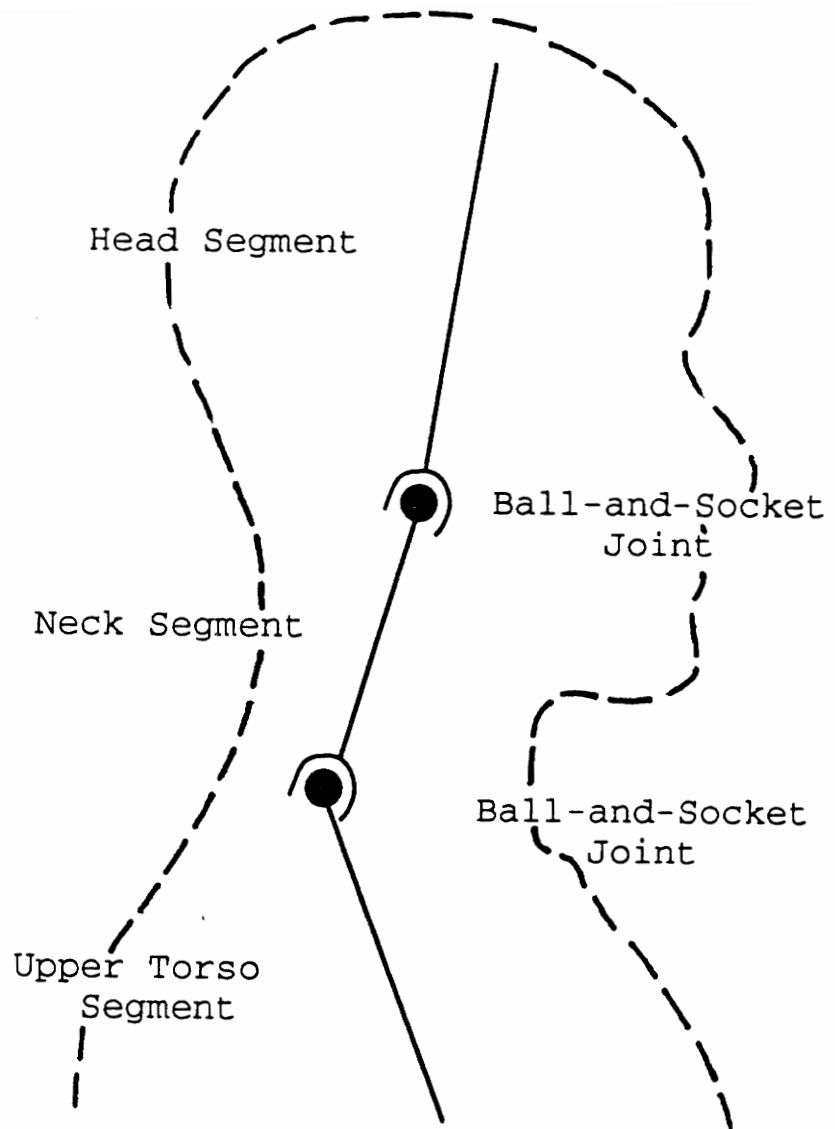


Figure 4.3 Three Segment/Two Ball-and-Socket Joint Model of Head/Neck System

occipital joint (skull-C1 articulation) and the twisting motion of the head on the neck allowed by the central atlanto-axial joint (C1-C2 articulation) are represented by a single ball-and-socket joint connecting the rigid head segment to the top of the neck segment. The location of the ball-and-socket joint geometrically correlates with the anatomical occipital condylar point of the skull. The motion of the neck derived from rotation or sliding between pairs of cervical discs is collectively represented by a second ball-and-socket joint connecting the neck segment to the top of the upper torso segment. This joint location correlates with the vertebral C7-T1 articulation.

Ball-and-socket joints allow total rotational freedom, restricting only relative translational motion between segments at the joint location. However, muscles and ligaments attached to the body segments apply resistance to passive rotational motion of the body. There also exists a rotational limit due to anatomical constraints on the joint. The resulting rotational retarding torques are modeled by torsional springs and dashpots applied to the two ball-and-socket joints (Figure 4.4). The calculated resistive torques for each joint are included in the angular equation of motion which is the second system equation in the matrix equation [3-3].

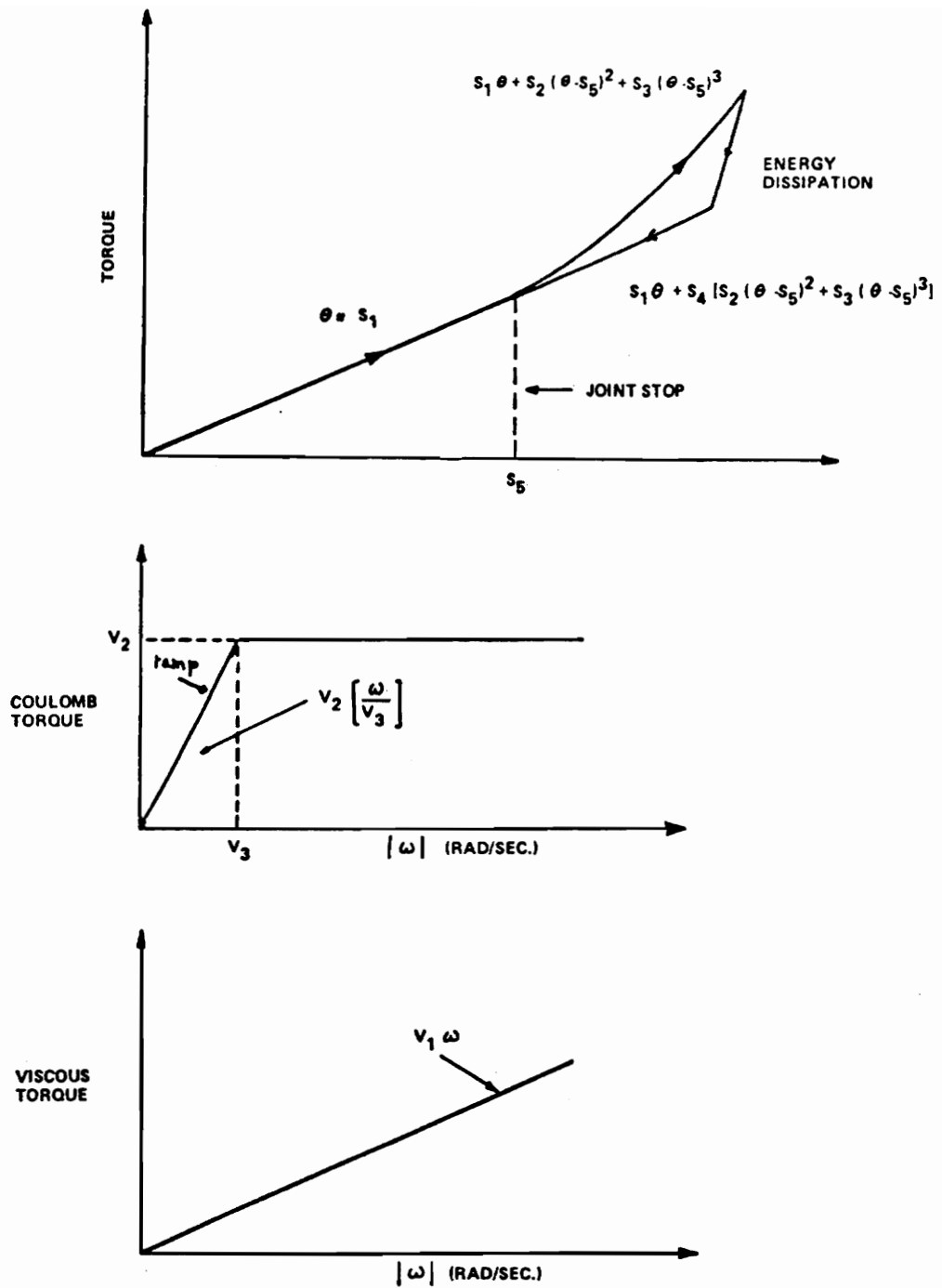


Figure 4.4 ATB Model Joint Spring, Coulomb, and Viscous Restoring Torque Functions

The magnitude of the spring torque  $T_{TOTAL}$  for each joint is governed by the equation:

$$T_{TOTAL} = \frac{T + T_s}{|\sin\theta|}, \quad [4-1]$$

where

$$T = S_1 |\theta| \quad [4-2]$$

and

$$T_s = \begin{cases} 0 & (\theta < S_s) \\ S_2(|\theta| - S_s)^2 + S_3(|\theta| - S_s)^3 & (\theta \geq S_s, d\theta/dt > 0) \\ S_4 T_s & (\theta \geq S_s, d\theta/dt < 0). \end{cases} \quad [4-3]$$

The variables in the above equations are defined as follows:

- $T_{TOTAL}$  = the total torsional resistance (in-lbs) of the joint to rotation,
- $T$  = the joint torque (in-lbs) due to muscles and ligaments,
- $T_s$  = the joint torque (in-lbs) due to the anatomical joint limit,
- $\theta$  = the relative angular displacement (deg) between joint Z-axes of the two joined segments,

$S_1, S_2, S_3$  = the linear, quadratic, and cubic torque coefficients (in-lbs/deg), (in-lbs/deg<sup>2</sup>), and (in-lbs/deg<sup>3</sup>), respectively,

$S_4$  = the energy dissipation coefficient (a dimensionless variable between 0 and 1), and

$S_5$  = the limiting joint stop angle (deg) with respect to the center of symmetry.

The direction of the spring torque vector is parallel to the direction of rotation. According to equation [4-1], and as illustrated in Figure 4.4, a linear resistive torque is applied as a function of the relative rotation of the joined segments until this rotation reaches the limiting joint stop angle. When the rotation reaches the joint stop angle, the applied torque increases as a cubic function to simulate the dramatic increase in joint resistance to rotation. An energy dissipation factor is included in the equation which decreases the amount of applied torque during unloading of the joint at angular displacements above the joint stop. This simulates the effect of energy absorption into the system.

The magnitude of the viscous and coulomb torques is governed by the equation:

$$\frac{T}{|\omega|} = V_1 + \frac{V_2}{\max(|\omega|, V_3)} \quad [4-4]$$

where

$\max(a, b)$  = the greater value: a or b,

$T$  = the resistance (in-lb) to rotation due to rate of relative segment rotation,

$|\omega|$  = the magnitude of the relative angular velocity (deg/sec) between the two jointed segments,

$V_1$  = the linear viscous coefficient (in-lb-sec/deg),

$V_2$  = the coulomb friction coefficient (in-lb), and,

$V_3$  = the relative angular velocity (deg/sec) of the joint at which full coulomb friction is applied.

The direction of the viscous and coulomb torque vectors is the same as that of the spring torque.

The values used for the resistive torque coefficients in current whole body simulations with the ATB model (given in Chapter 5.2) were validated for use with simulations of human response to  $-G_x$  and  $+G_y$  accelerations where large head rotations have been observed. This three rigid segment/two ball-and-socket joint characteristic of the human head/neck system is not well suited for simulations of human response to

ejection accelerations. The available resistive torque coefficients have not been validated for use with simulations of human response to  $+G_z$  accelerations. Moreover, there is no mechanism in the  $-G_x$  and  $G_y$  impact response characterization for representing the axial deformation of the cervical spine exhibited experimentally when the head/neck system is subjected to vertical accelerations (for example see Chapter 5.1).

The objective of the study described herein is to develop, within the constraints of the three dimensional, rigid body Articulated Total Body Model, predictive computer simulations of human head and neck system responses to an ejection environment. Specifically, this thesis addresses modifications of the current three segment/two ball-and-socket joint head/neck characterization necessary to reproduce experimentally measured human head/neck responses to a  $+10 G_z$  acceleration pulse.



## 5.0 Solution Methods

### 5.1 Live Human Subject Simulations

Nine male military personnel participated in live human subject testing conducted at Armstrong Laboratory to evaluate the effects of Night Vision Goggles (NVG's) on human response during ejection accelerations (3). The test facility for the study was the Vertical Deceleration Drop Tower illustrated in Figure 5.1. Test Cell A required a seated subject, equipped with an HGU-26/P helmet and a MBU-5/P mask (no NVG's) to be subjected to a 10  $G_z$  deceleration exposure, which produces an acceleration exposure similar to that of an ACES II ejection seat.

By allowing the test seat carriage of the Deceleration Tower to free-fall vertically under the support of a guide rail system, and impact against a hydraulic deceleration device, the test seat and the subject were rapidly decelerated. The downward deceleration is dynamically equal to an upward acceleration of the same magnitude and thus is representative of ejection acceleration. The profile of the deceleration is produced by a plunger attached to the undercarriage of the test seat. Upon impact with the

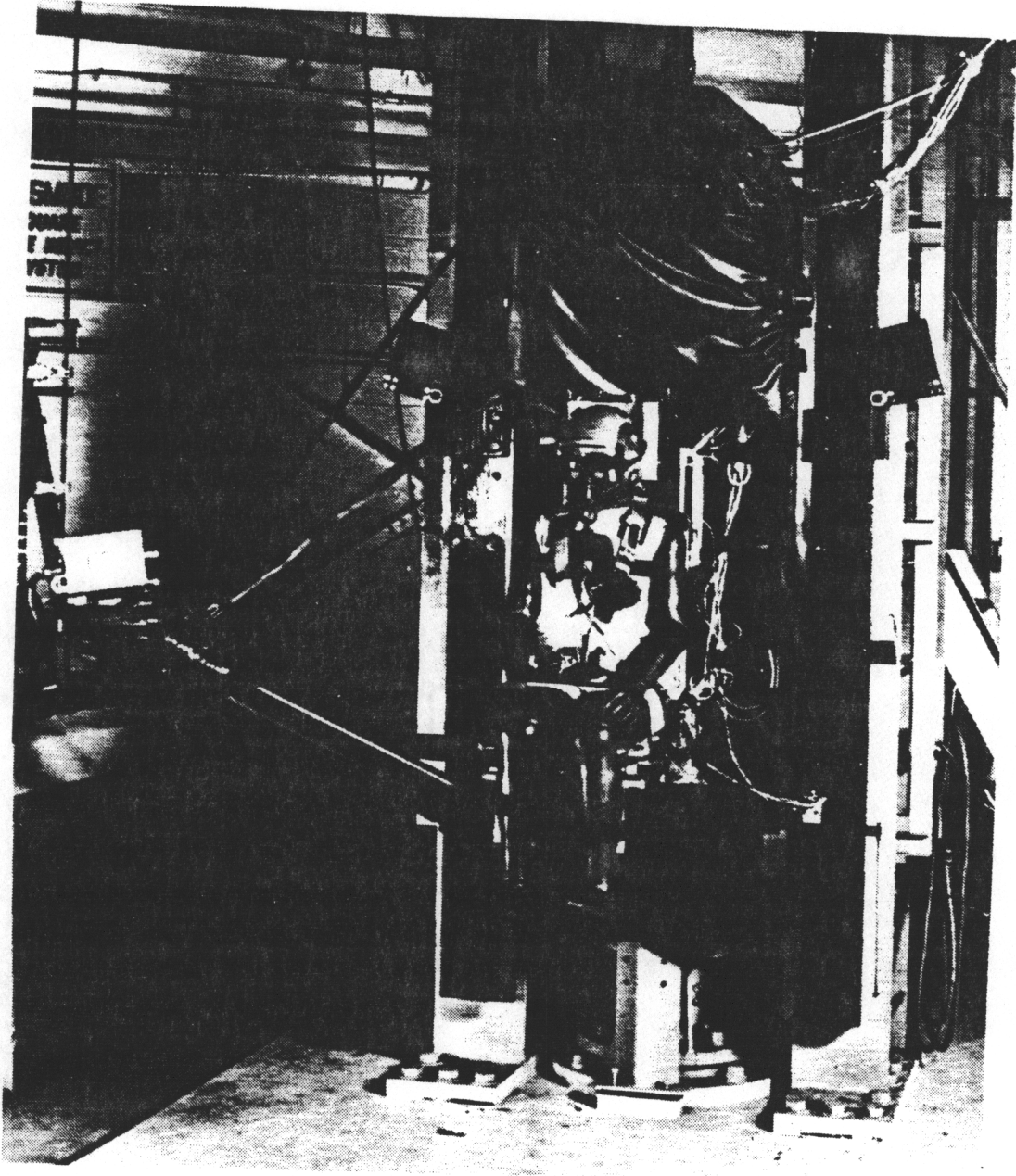
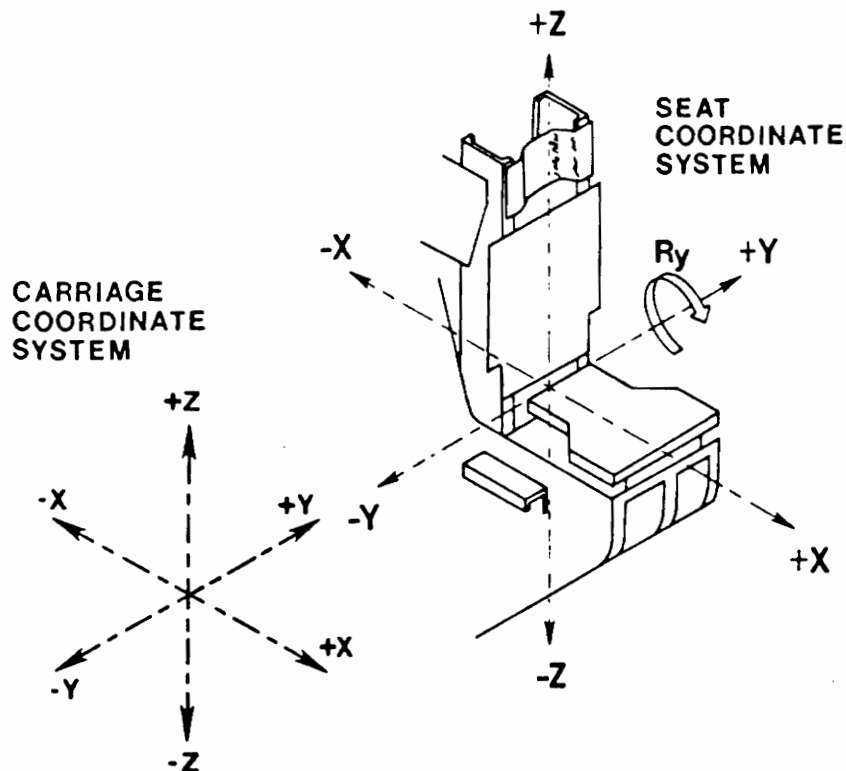


Figure 5.1 AAMRL Vertical Deceleration Drop Tower

hydraulic decelerator, the plunger displaces water in a filled cylinder located at the bottom of the tower. The shape of the plunger, the diameter of the cylinder, and the initial carriage height determine the shape of the deceleration profile.

The test accelerometer coordinate system defined with respect to the test seat is shown in Figure 5.2. The Z-axis is parallel to the seat back and positive in the buttocks-to-head direction for the seated subject. This is in the opposite direction of the ATB model Z-axis. The X-axis of the test accelerometer coordinate system is perpendicular to the Z-axis and positive in the eyes forward direction for the seated subject. The Y-axis is perpendicular to the Z- and X-axes according to the right hand rule.

The carriage deceleration is illustrated in Figure 5.3. The data has been adjusted using computer processing software to remove the constant -1 G effect of gravity. This results in a profile which describes the seat deceleration with respect to a local reference frame. Time zero milliseconds on Figure 5.3 marks the point of impact with the deceleration device, while the period preceding zero (-145 to 0 ms) indicates the period of free fall, and the time following zero (0 to 500 ms) indicates the local deceleration with respect to time.



1. ALL TRANSDUCERS EXCEPT THE CARRIAGE ACCELEROMETERS AND THE CARRIAGE VELOCITY TACHOMETER WERE REFERENCED TO THE SEAT COORDINATE SYSTEM. THE CARRIAGE TACHOMETER WAS WIRED TO PROVIDE A POSITIVE OUTPUT VOLTAGE DURING FREEFALL. THE CARRIAGE ACCELEROMETERS WERE REFERENCED TO THE CARRIAGE COORDINATE SYSTEM.
2. THE LINEAR ACCELEROMETERS WERE WIRED TO PROVIDE A POSITIVE OUTPUT VOLTAGE WHEN THE ACCELERATION EXPERIENCED BY THE ACCELEROMETER WAS APPLIED IN THE  $+x$ ,  $+y$  OR  $+z$  DIRECTION AS SHOWN.
3. THE ANGULAR  $R_y$  ACCELEROMETERS WERE WIRED TO PROVIDE A POSITIVE OUTPUT VOLTAGE WHEN THE ANGULAR ACCELERATION EXPERIENCED BY THE ANGULAR ACCELEROMETER WAS APPLIED IN THE  $+y$  DIRECTION ACCORDING TO THE RIGHT HAND RULE AS SHOWN.

Figure 5.2 Accelerometer Coordinate System for Vertical Deceleration Drop Tower Test

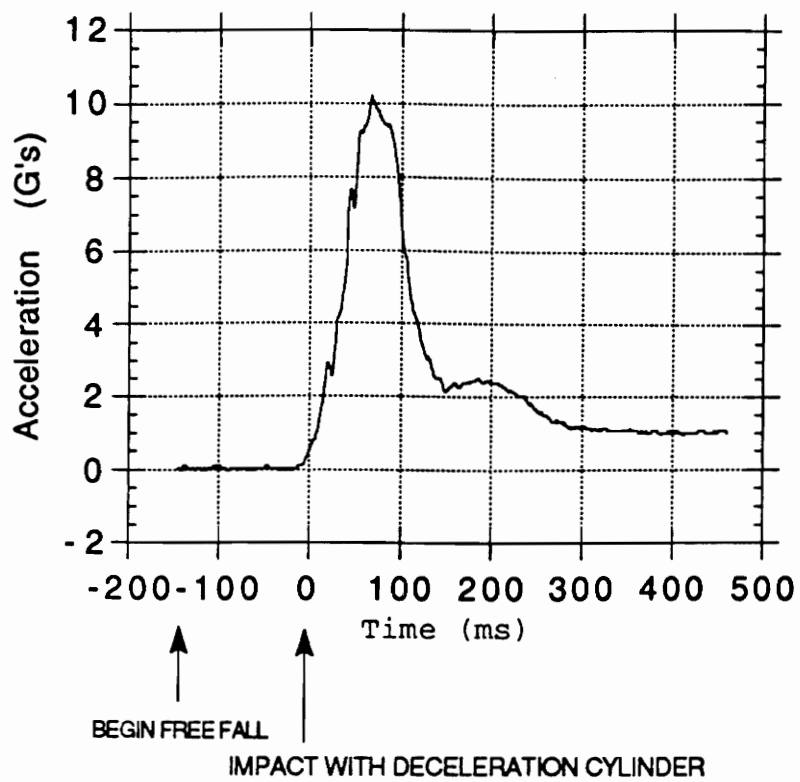


Figure 5.3 Measured Carriage Acceleration for Human Drop Tower Test

The decelerations of the seat, the carriage, and the head and chest of the subject were recorded throughout the test. The X, Y, and Z linear decelerations and the angular acceleration,  $R_Y$ , about the Y-axis were measured for the subjects' chest by accelerometers mounted to a chest block, covered by a steel protection shield and fastened at the sternum by a Velcro strap. The same accelerations for the head were measured by a set of four accelerometers mounted to the external edge of a plastic dental bite block inserted into the mask.

The chest and head decelerations for subject L7 are shown in Figures 5.4 and 5.5, respectively, filtered of frequencies above 50 Hz (noise). While there exists some response in the X and Y directions, 98.5% of the subject head and 99.0% of the subject chest maximum resultant response acceleration was in the Z-direction. The maximum chest deceleration for this subject was 11.26 G's in the Z-direction which is within the 11.20-15.20  $G_z$  envelope of the nine subjects. The maximum head deceleration for this subject was 15.66 G's in the Z-direction which is also within the 9-subject 14.69-19.48 G envelope. Thus, subject L7 is an appropriate "representative" of a typical human biodynamic response to the 10 G seat deceleration profile of Figure 5.3.

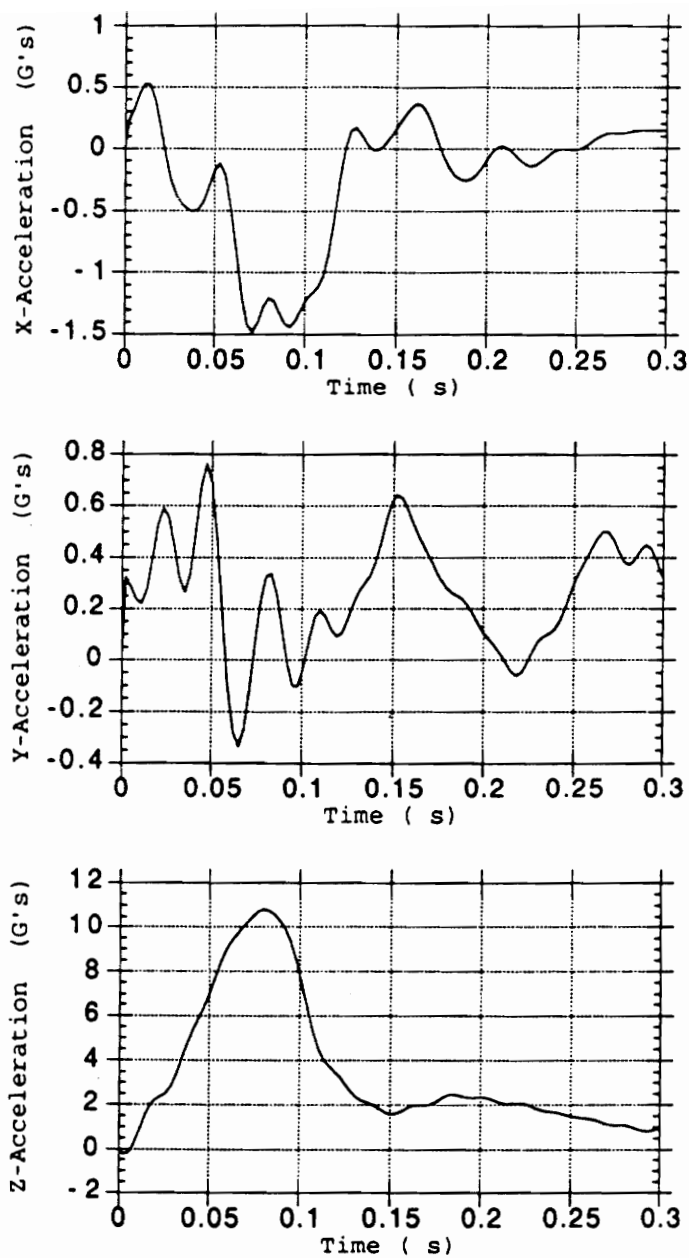


Figure 5.4 Measured Subject Chest Acceleration for Human Drop Tower Test (Filtered of 50 Hz and Above)

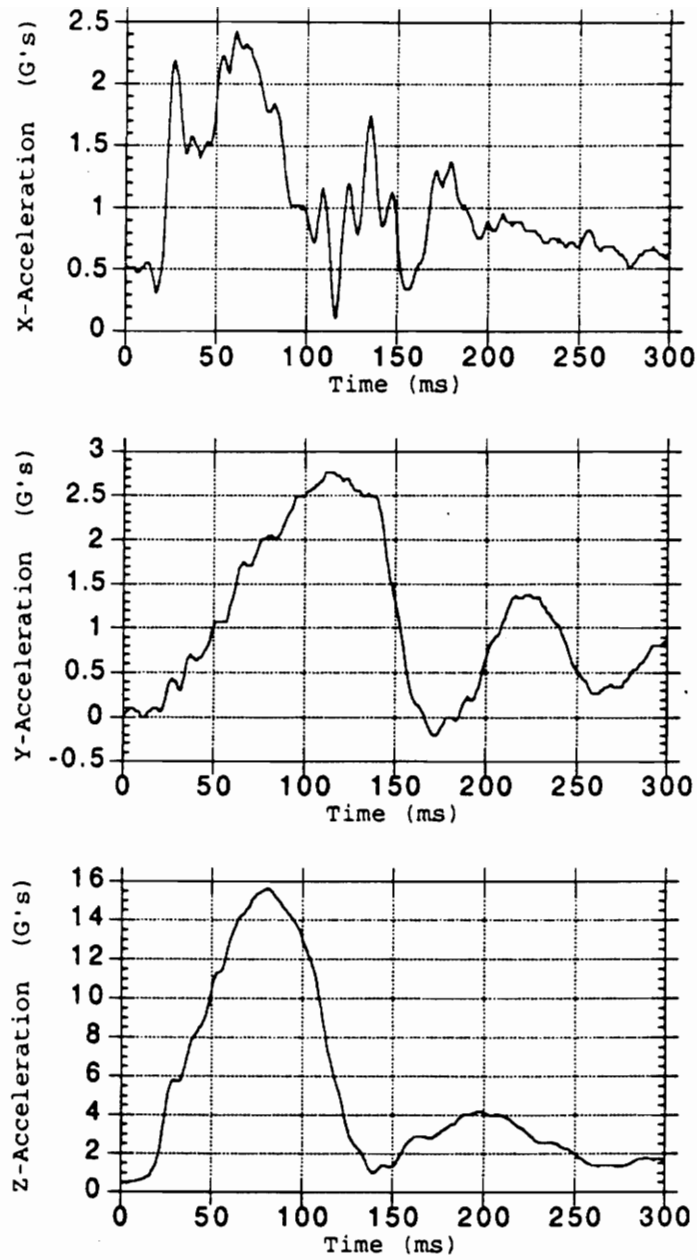


Figure 5.5 Measured Subject Head Acceleration for Human Drop Tower Test (Filtered of 50 Hz and Above)



Anthropometric data for each subject participating in the study had been previously obtained and was available from the Biodynamics Data Bank at the Armstrong Laboratory (17). Values for height, weight, head weight, head center of gravity, position of occipital condyle and head moments of inertia were compiled from the Data Bank for each individual. Calculated combined inertial properties of the subject head and the helmet/mask system were also provided. This data for subject L7 is presented in Table 5.1.

The human head data described above was measured in the anatomical coordinate system (3) (Figure 5.6) which is defined by anatomical landmarks visible on the head exterior. The four landmarks are the skin over the left and right infraorbital notches, which are anatomical points located just below each eye socket (16), and the superior edge of the left and right external auditory meati, which are anatomical points located at the top of each ear canal opening. The anatomical Y-axis is defined by the line connecting the left and right external auditory meati. The line perpendicular to the Y-axis and passing through the midpoint of the left and right infraorbital notches forms the X-axis. The Z-axis is perpendicular to the X-Y plane according to the right hand rule.

Two onboard high-speed LOCAM cameras, operating at 500 frames per second, were used to produce photogrammetric data

Table 5.1      Anthropometric Data for Subject L-7

|   |                           |                          |                          |
|---|---------------------------|--------------------------|--------------------------|
| general                                 |                           |                          |                          |
| height (in)                             | 68.8                      |                          |                          |
| weight (lbs                             | 150                       |                          |                          |
| head                                    |                           |                          |                          |
| weight (lbs)                            | 9.3                       |                          |                          |
| center of gravity (in)                  | -0.01                     | 0.03                     | 1.12                     |
| principal moments (lb-in <sup>2</sup> ) | 68.21                     | 79.55                    | 50.54                    |
| direction cosines                       | 0.807<br>-0.065<br>-0.586 | 0.053<br>0.998<br>-0.038 | 0.587<br>0.000<br>0.809  |
| occipital condyle (in)                  | -1.04                     | 0.0                      | -1.22                    |
| head/helmet/mask                        |                           |                          |                          |
| weight (lbs)                            | 13.06                     |                          |                          |
| principal moments (lb-in <sup>2</sup> ) | 145.9                     | 150.8                    | 116.5                    |
| direction cosines                       | 0.759<br>-0.556<br>0.3384 | 0.571<br>0.818<br>-0.065 | 0.313<br>-0.144<br>0.939 |
| center of gravity (in)                  | -0.135                    | 0.063                    | 0.912                    |

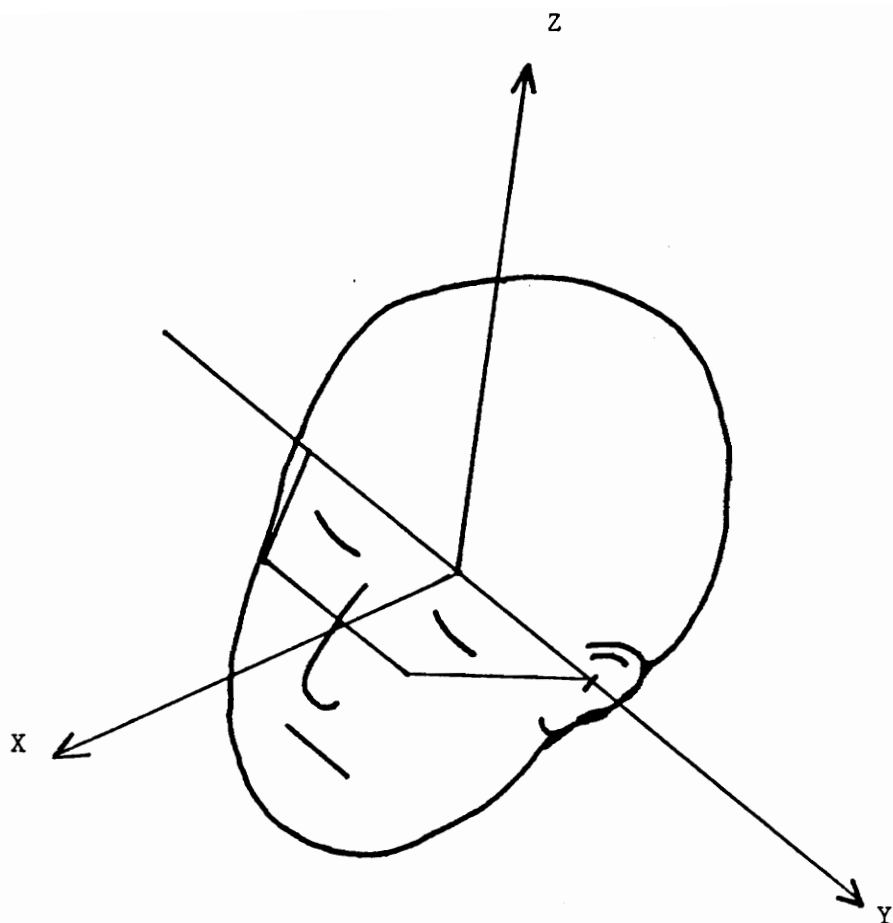
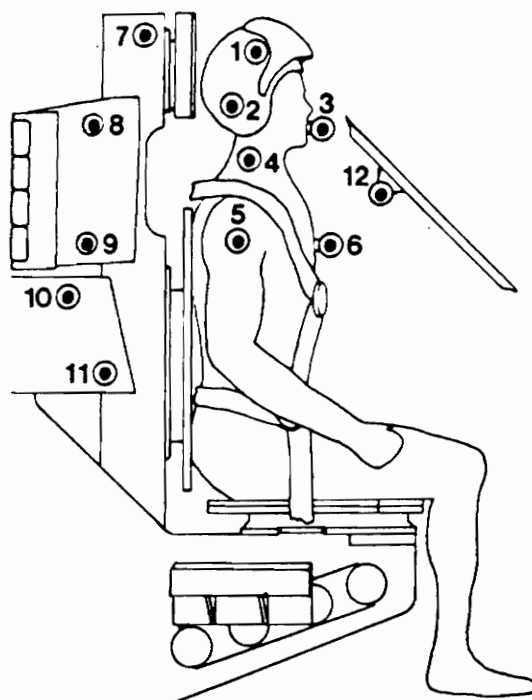


Figure 5.6 Anatomical Coordinate System for the Human Head

of the subject motion during the test. Motion of the subject's helmet, mask, neck, shoulder and chest was quantified from these films by tracking the motion of subject-mounted fiducials (0.75" diameter black circle on a 1.25" diameter target) (Figure 5.7). The resultant velocity and displacement data obtained for subject L7's chest and head are shown in graphical form in Figures 5.8 and 5.9. The displacement data shows a maximum chest displacement to be 0.544" at 86 ms in the Z-direction and a maximum mask displacement to be 1.585" at 94 ms in the Z-direction. This results in a maximum potential displacement between the mask and the chest of about 1.1 inches in the Z-direction (the displacement in the X- and Y-directions was negligible). This data illustrates that head rotation is minimally involved in the response mechanism for the head and neck when a subject is exposed to a 10  $G_z$  acceleration.

## **5.2 Computer Ejection Simulations with Current ATB Head/Neck Analog**

The experimental results compiled from human subject L7 (height 68.8 inches, weight 150 lbs.) were chosen to validate a preliminary ATB simulation of the corresponding + $G_z$  impact profile. The three rigid segment/two ball-and-socket joint



ALL DIMENSIONS ARE REFERENCED TO THE SEAT REFERENCE POINT (SRP).  
THE SEAT REFERENCE POINT IS LOCATED AT THE INTERSECTION OF THE  
SEAT PAN CENTER LINE AND THE SEAT BACK CENTER LINE (Z AXIS).

0 DEGREE SEAT POSITION

| DESCRIPTION            | DIMENSIONS IN FEET |         |         |
|------------------------|--------------------|---------|---------|
|                        | X                  | Y       | Z       |
| 1. UPPER HELMET        | -                  | -       | -       |
| 2. LOWER HELMET        | -                  | -       | -       |
| 3. MASK                | -                  | -       | -       |
| 4. NECK                | -                  | -       | -       |
| 5. SHOULDER            | -                  | -       | -       |
| 6. CHEST               | -                  | -       | -       |
| 7. UPPER FRAME         | -0.1411            | -0.5399 | +3.3953 |
| 8. UPPER NUMBER PLATE  | -0.7979            | -0.7887 | +2.6854 |
| 9. LOWER NUMBER PLATE  | -0.8225            | -0.7904 | +1.8163 |
| 10. CENTER FRAME       | -0.6312            | -0.6337 | +1.4196 |
| 11. LOWER CENTER FRAME | -0.3632            | -0.6616 | +0.8258 |
| 12. CAMERA STRUT       | +2.0518            | -2.4725 | +2.3162 |

Figure 5.7 Subject Mounted Fiducial Location for Human Test  
Photogrammetric Data

NVGI STUDY TEST: 1770  
SUBJ: L-7 CELL: A

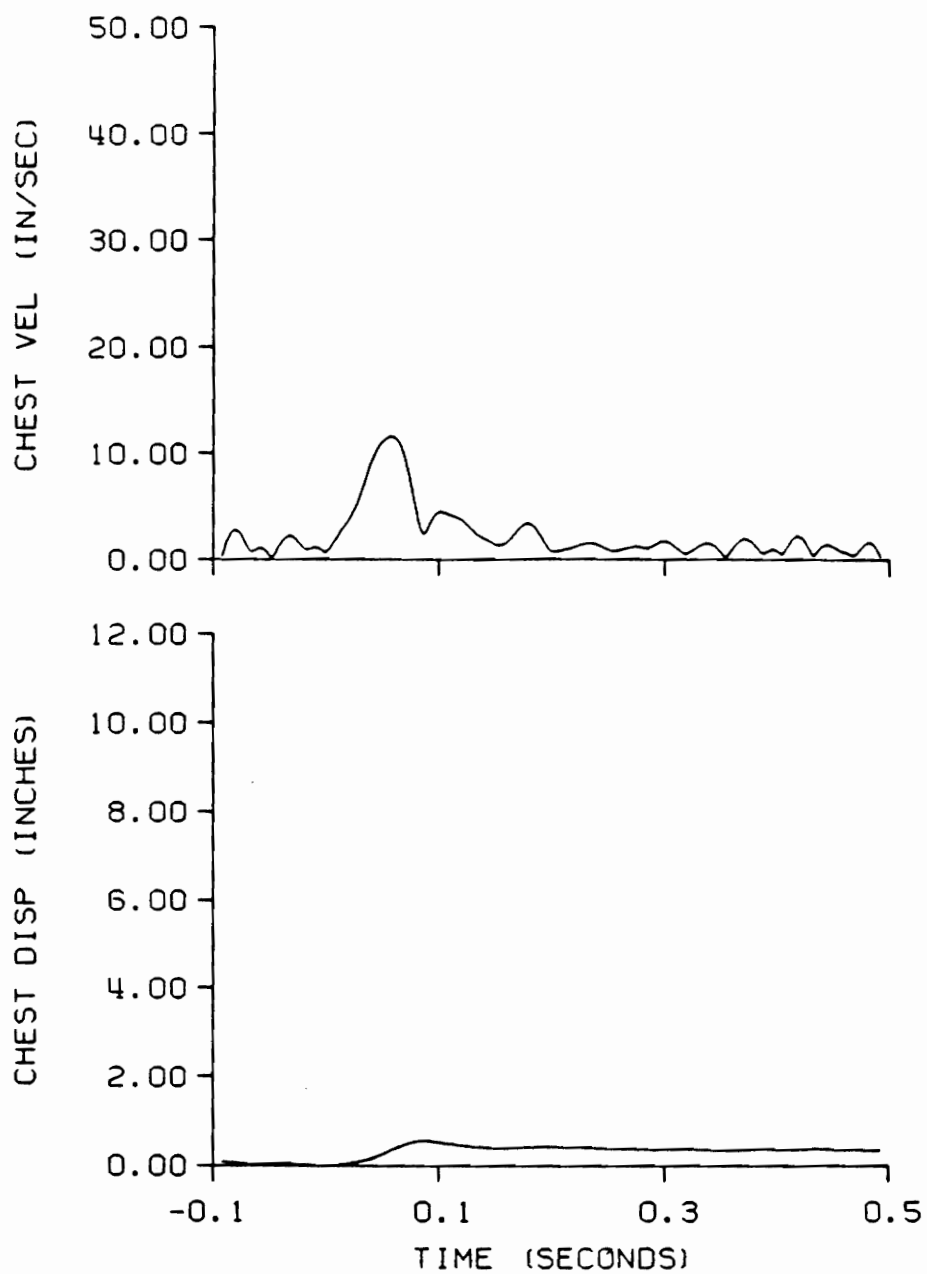


Figure 5.8 Test Subject L7 Chest Photogrammetric Data

NVGI STUDY TEST: 1770  
SUBJ: L-7 CELL: A

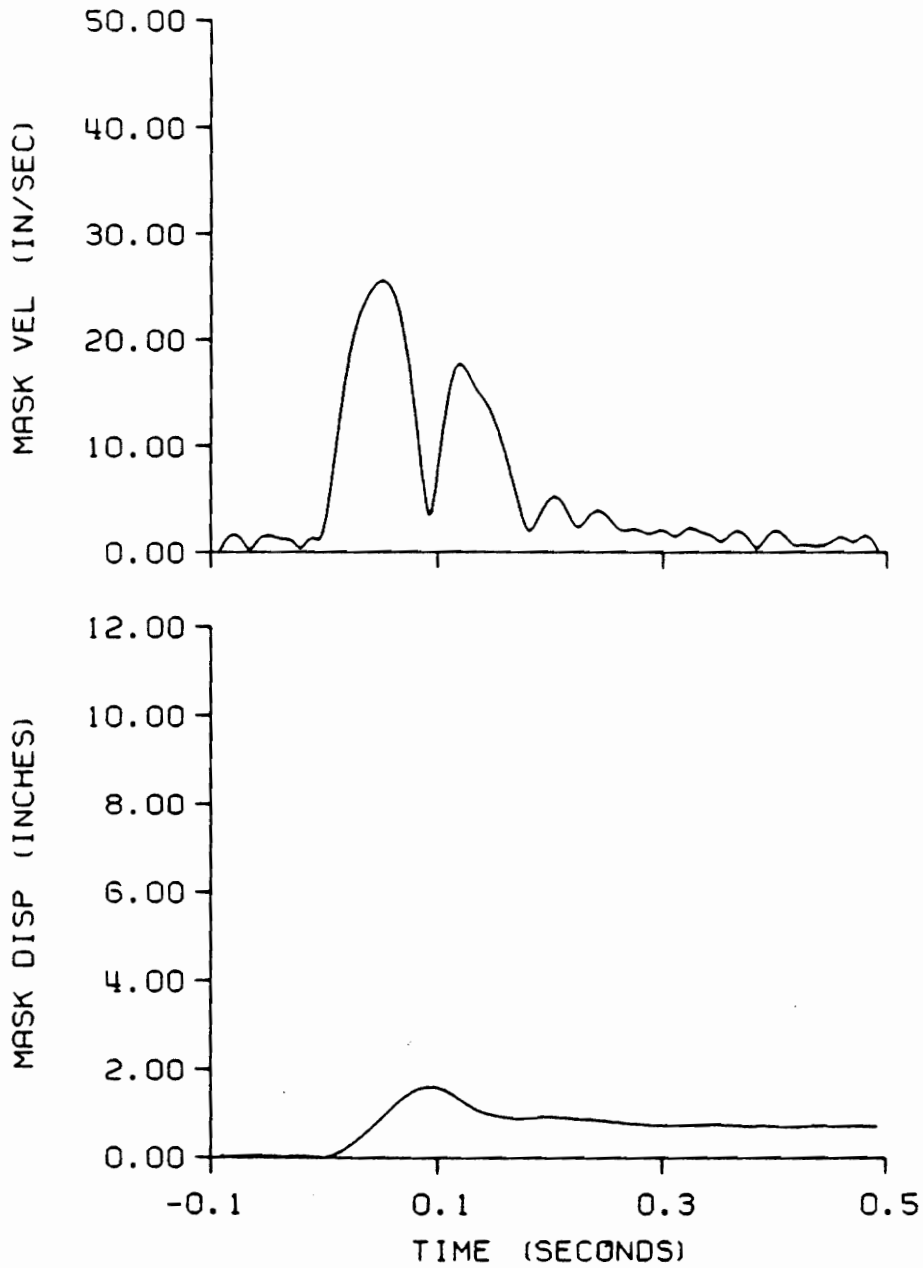


Figure 5.9 Test Subject L7 Head Photogrammetric Data

model of the head and neck described in Chapter 4.2 was used with the ATB model to create this simulation. The physical characteristics of the three rigid body segments used as input to the model were a combination of the measured anthropometric data for subject L-7 and statistical adult human male anthropometric data and are illustrated in Figure 5.10.

The head segment of the model represents the combination of the human head and the helmet/mask system. Thus, the head segment weight used in the simulation (13.06 lbs) was the sum of the measured head weight for subject L-7 (9.43 lbs) and the measured weight of the helmet/mask system (3.63 lbs). The combined center of gravity, (-0.1351, 0.0634, 0.9115) measured in anatomical coordinates (defined in Chapter 5.1), was the center of gravity for the head segment. The combined head-helmet-mask inertial tensor, measured in anatomical coordinates, was transformed to the head segment local coordinate system, diagonalized to produce principal moments, and put into ATB model input format [see Appendix A]. The resulting principal moments of inertia

$$I_H = \begin{Bmatrix} I_X \\ I_Y \\ I_Z \end{Bmatrix} = \begin{Bmatrix} 0.3550 \\ 0.3575 \\ 0.3006 \end{Bmatrix} \text{ lbs-sec}^2\text{-in}, \quad [5-1]$$

which are rotated 25 degrees about the head local Y-axis, were used to define the inertial properties of the head segment in the ATB model.



Figure Not to Scale  
Dimensions in Inches

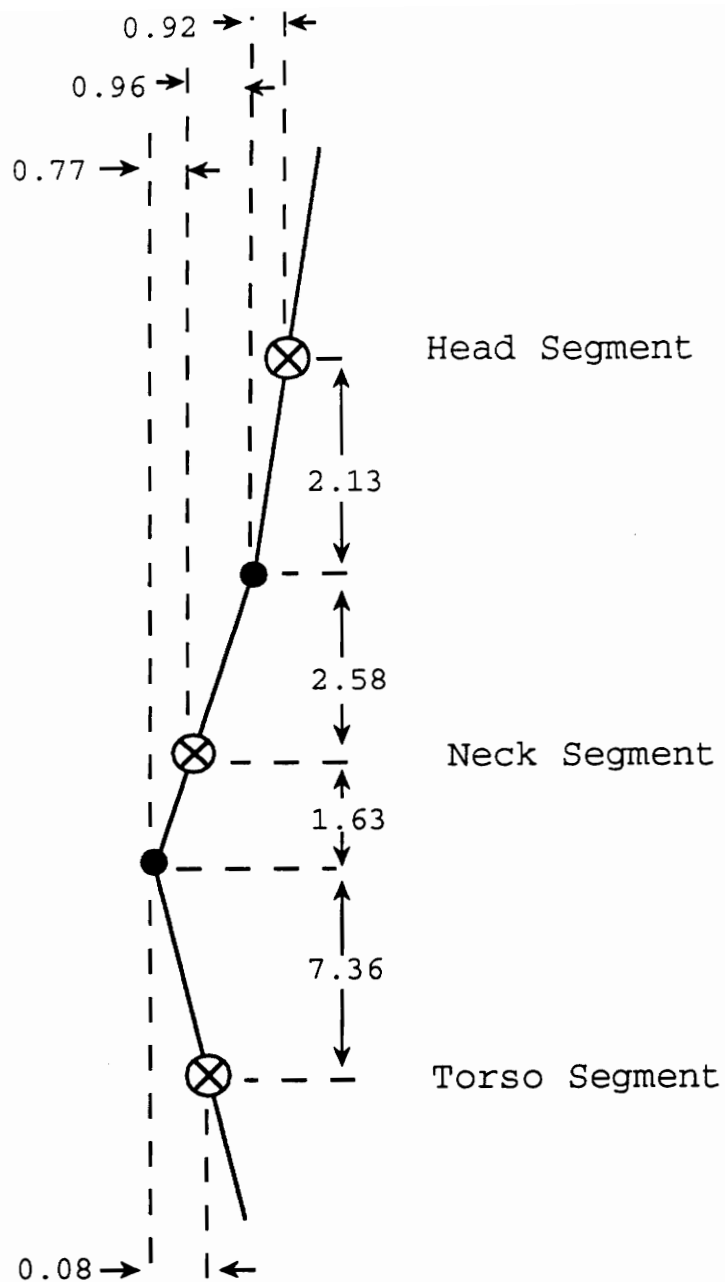


Figure 5.10 Physical Measurements of Human Head/Neck Model

The location of the upper neck joint relative to the head segment center of gravity was defined as the location of the occipital condylar point of the subject measured in anatomical coordinates. The resulting location of the upper neck joint was defined by the vector:

$$\vec{r}_H = -0.92\vec{i}_H + 0.0\vec{j}_H + 2.13\vec{k}_H \quad [5-2]$$

where the subscript H designates the head local coordinate system, and  $(\vec{i}, \vec{j}, \vec{k})$  represents the (X, Y, Z) unit vectors.

The remainder of the physical characteristics for the head, neck and upper torso were obtained using the GEBODIII program. GEBODIII, GEnerator of BOdy Data, is a program provided with the ATB model which uses regression analysis based on whole body height and/or weight to provide the physical body property data for ATB model simulations. This data includes the physical characteristics of the body segments such as the segment weight and moments of inertia, and the physical characteristics of the joints such as the joint location, the type of joint, the joint spring function coefficients, and the joint viscous function coefficients. The data for this head/neck system simulation was from regression analysis of data sets of adult human male Air Force Flying Personnel based on subject L-7's 68.8 inch height and

150 lb weight. The GEBODIII data was used only where directly measured data was unavailable.

The weights for the neck and the upper torso were 1.99 lbs and 44.7 lbs, respectively. The principal moments of inertia  $I_N$ , for the neck were:

$$I_N = \begin{Bmatrix} I_X \\ I_Y \\ I_Z \end{Bmatrix} = \begin{Bmatrix} 0.0124 \\ 0.0150 \\ 0.0183 \end{Bmatrix} \text{ lbs-sec}^2\text{-in}, \quad [5-3]$$

which are not rotated in the neck local coordinate system, and the principal moments of inertia  $I_T$  for the upper torso were:

$$I_T = \begin{Bmatrix} I_X \\ I_Y \\ I_Z \end{Bmatrix} = \begin{Bmatrix} 3.3356 \\ 2.4325 \\ 2.0262 \end{Bmatrix} \text{ lbs-sec}^2\text{-in}, \quad [5-4]$$

which are rotated 14.4 degrees about the torso local Y-axis.

The location of each joint is described in the local coordinate system of the two segments by the vectors  $\vec{r}_j$ . The location of the lower neck joint at the C7-T1 articulation was defined by the vectors:

$$\vec{r}_T = -0.08\vec{i}_T + 0.0\vec{j}_T - 7.36\vec{k}_T \quad [5-5]$$

relative to the torso segment local coordinate system, and

$$\vec{r}_N = -0.77\vec{i}_N + 0.0\vec{j}_N + 1.63\vec{k}_N, \quad [5-6]$$

relative to the neck segment coordinate system, where the subscript T designates torso and the subscript N designates neck. The location of the upper neck joint with respect to the neck C.G. was defined by the vector:

$$\vec{r}_N = 1.01\vec{i}_N + 0.0\vec{j}_N - 2.54\vec{k}_N. \quad [5-7]$$

As explained in Chapter 4.2, the rotational retarding forces from passive muscle response and ligament constraints are modeled by torsional springs and dampers applied at the joint location parallel to the direction of rotation. The magnitude of the flexure torque is computed using Equation [4-1] and joint spring function coefficients, and the magnitude of the viscous and coulomb torques are computed using Equation [4-4] and viscous function coefficients. Since these coefficients can not be directly measured for the test subject, the currently accepted values provided by the GEBODIII program were used as first approximations. The flexure spring coefficients used in this simulation are given in Table 5.2. The joint stop, or maximum rotation the human joint will allow, was 25 degrees relative rotation for both of the ball-and socket joints. The viscous coefficient for this model was 0.1, while no coulomb torque was applied.

The model was driven by acceleration applied to the center of gravity of the upper torso segment. The

Table 5.2                      Joint Flexure Spring Coefficients

---

|                                |                        |     |
|--------------------------------|------------------------|-----|
| Linear Spring Coefficient      | in-lb/deg              | 0.0 |
| Quadratic Spring Coefficient   | in-lb/deg <sup>2</sup> | 5.0 |
| Cubic Spring Coefficient       | in-lb/deg <sup>3</sup> | 0.0 |
| Energy Dissipation Coefficient | dimensionless          | 0.7 |
| Joint Stop Location            | degrees                | 25  |

---

experimentally measured chest X, Y, and Z linear acceleration data shown in Figure 5.3 for subject L7 were used as the driving input acceleration into the computer model. The assumption that the linear accelerations measured at the chest are equivalent to those at the center of gravity of the upper torso was based on the negligible angular rotation of the chest. Thus the upper torso moves as a rigid body without rotation and is presumed to have the same acceleration on any point on the body. The maximum rotation of the chest about the local Y-axis, obtained by integrating chest angular accelerometer data, was 0.05 degrees.

Comparison of the results generated by this simple rigid segment/two ball-and-socket joint model with those corresponding to the actual human response mechanism showed that the model neck characterization is not adequate for simulating the human head/neck response to  $+G_z$  accelerations (See Chapter 6). The axial forces on the cervical column from the buttocks-driven  $+10 G_z$  impact acceleration primarily compress the neck. Compression of the neck decreases the distance between the atlanto-occipital joint and the C7-T1 joint. Under this compressive action the head accelerates toward the torso with minimal rotation ( $\pm 0.05$  degrees). This response mechanism produces head acceleration due to head translation in the  $+Z$  direction. The current ATB head/neck

model characterizes rotation between the segments and thus could simulate head or neck rotation. However, no mechanism exists in the head/neck model to characterize axial deformation. Thus, it is not possible to simulate the head translational response to axial neck compression. Without the provision for neck compression in the head/neck characterization, the computerized ATB model cannot generate biodynamic simulations suitable for predicting the human head/neck system response to  $+G_z$  accelerations.

### **5.3 Computer Ejection Environment Simulations with Proposed ATB Head/Neck Analog**

The axial compression of the neck described in Section 5.2 must be incorporated into the rigid body model of the head/neck system to improve the simulation of human response to Z-acceleration. This improvement was accomplished in this study by replacing the ball-and-socket joint that connects the neck and upper torso with a "slip joint". The slip joint allows the neck segment to linearly displace or slide with the torso segment (see Figure 5.11). Such sliding will produce a decrease in the distance between the atlanto-occipital joint located at the head/neck articulation and the C7-T1 neck joint located at the neck/torso articulation; thus simulating, using

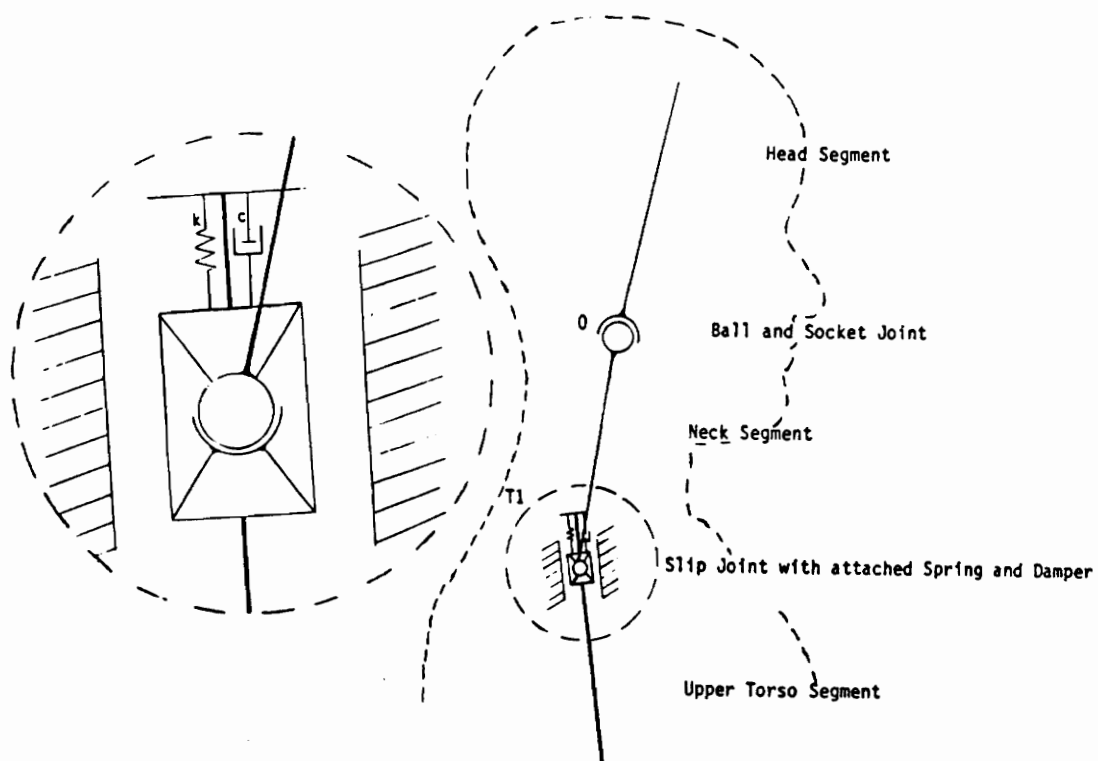


Figure 5.11 Three Segment/Ball-and-Socket and Slip Joint  
Viscoelastic Head/Neck Model



rigid-body mechanics, the decreased distance between the joints caused by neck compression.

The replacement of the ball-and-socket joint with a slip joint at the lower neck articulation necessitates modifying the linear position constraint equation [3-4]. The location of the joint with respect to the neck segment center of gravity is constant and is thus unchanged from Equation [3-4], described in inertial coordinates as  $\vec{x}_N + D_N^{-1} \vec{r}_{Nj}$ . However, the location of the joint with respect to the torso segment center of gravity changes as the neck segment slides along the torso. Thus, the location of the joint with respect to the upper torso center of gravity changes from  $\vec{x}_T + D_T^{-1} \vec{r}_{Tj}$  to  $\vec{x}_T + D_T^{-1} (\vec{r}_{Tj} + \vec{d})$  where  $\vec{d}$  is the displacement of the joint from the original position  $\vec{r}_T$ . The resulting linear position constraint equation for the slip joint (23) is:

$$\vec{x}_T + D_T^{-1} (\vec{r}_{Tj} + \vec{d}) = \vec{x}_N + D_N^{-1} \vec{r}_{Nj} \quad [5-8]$$

The displacement vector  $\vec{d}$  is constrained to lie along the local Z-axis of the torso segment.

The amount and rate at which the neck segment slides along the upper torso segment can be controlled by specifying a spring and viscous damper characteristic for the C7-T1 slip joint. By attaching the ends of the spring and damper to the neck segment and the torso segment at the original joint location,  $\vec{r}_N$  and  $\vec{r}_T$  respectively, the spring force  $\vec{F}_{spring}$  is

a function of the displacement  $\vec{d}$  which is defined by Equation [5-8]. Then

$$\vec{F}_{spring} = k_1 \vec{d} + k_2 |\vec{d}^2|, \quad [5-9]$$

and the damping force  $\vec{F}_{damper}$  is a function of the rate of this displacement

$$F_{Damper} = c \dot{d}. \quad [5-10]$$

The spring force is assumed to be a quadratic function of the spring displacement to simulate in the simplest form the nonlinear behavior for the compression of the neck. Since little documentation is available on the exact damping properties of the neck, the damping force is modeled in this simulation as a simple linear damper.

The viscoelastic properties  $k_1$ ,  $k_2$ , and  $c$  of the Voigt spring and damper model were determined in this study by optimizing the correlation between computer-predicted model responses and measured empirical data. Sets of simulations were produced by varying  $k_1$  from 0 to 100 lbs/in, varying  $k_2$  from 0 to 250 lbs/in<sup>2</sup>, and varying  $c$  from 0 to 10 lb-sec/in, as presented in Table 5.3. The experimental data from the Vertical Drop Tower Tests suggested that the system response

Table 5.3      Spring and Damping Coefficients for  
Neck/Torso Slip Joint Used in ATB  
Simulations

| Spring Coefficients |                    | Damping Coefficient |
|---------------------|--------------------|---------------------|
| $k_1$               | $k_2$              | $c$                 |
| lb/in               | lb/in <sup>2</sup> | lb-sec/in           |
| 0                   | 0                  | 0.5                 |
| 50                  | 50                 | 1.0                 |
| 100                 | 100                | 1.5                 |
|                     | 150                | 2.0                 |
|                     | 200                | 2.5                 |
|                     | 250                | 5.0                 |
|                     |                    | 10.0                |

was slightly underdamped. Values of  $c$  were chosen to converge on a damping coefficient for which the magnitude of the maximum acceleration, the time following the onset of the  $G_z$  response at which this maximum acceleration occurs, and the phase of the profile, all matched experimentally-measured data. The experimental data suggested that the stiffness of the head/neck model should be such that there will be no more than about a one-inch displacement of the head at the point of maximum excursion. Values of  $k_1$  and  $k_2$  were chosen to converge on spring coefficients for which the magnitude of the relative displacement between the head and torso segments matched the experimentally-measured value.

To remove the effect of head rotation and the unknown resisting torques generated actively or passively in the head, the segments were restricted from any relative rotational motion at the joints. This degree of freedom may be reintroduced to the model later for simulations of head and neck response to acceleration which include head rotation.

## 6.0 Results and Discussion

Computer simulations of human dynamic response to acceleration were created using three different characteristics to represent the human head and neck system: (i) the original three rigid segment/two ball-and-socket joint "simple" head/neck analog; (ii) the same analog with resisting torques added to the joints to simulate muscle and ligament constraints; and (iii) a three segment/two joint model with a viscoelastic slip joint (Figure 5.11) replacing the ball-and-socket joint at the neck/torso articulation.

The objective of this project was to characterize neck properties which produce a dynamic response simulating measured human biodynamic response to a 10  $G_z$  acceleration pulse. The measured human response used to evaluate these simulations was that of subject L7, who participated in the Vertical Deceleration Drop Tower Test at the Armstrong Laboratory. The photogrammetric and accelerometer data presented in Chapter 5.1 was used to qualitatively and quantitatively evaluate the results of the aforementioned simulations. The results of all of the simulations and comparisons with the measured data are presented in terms of the human test seat inertial coordinate system shown in Figure

5.2. All of the Z-direction simulation response curves have been shifted by 1 G to accommodate a 1  $G_z$  addition to the response by the ATB model.

The simulations were first evaluated qualitatively by comparing the response mechanism of the subject to that of the three rigid segments. The high speed films of the drop tower test show the subject to be stiff (i.e. muscles contracted) during the test and to respond to the impact with very little motion. The subject's head and chest do not appear to rotate. However, the neck compress during the impact.

The measured head acceleration response for Subject L7 is shown in Figure 5.5. The maximum head response acceleration in the Z-direction was 15.66 G's at 81 ms. The maximum head acceleration in the X- and Y-directions were only 2.43 G's at 61 ms and 2.76 G's at 111 ms, respectively (about 15% to 18% of the Z-acceleration). It was noted in Chapter 5.1 that 98.5% of the subject maximum resultant head response was in the positive Z-direction. Thus, the primary criterion for evaluating the simulated response was how well the Z-direction head acceleration profiles correlated with the corresponding measured head acceleration. Specifically, the evaluation was based on the magnitude of the maximum acceleration predicted, compared to 15.66 G's measured maximum, the predicted time at which that acceleration was reached compared to measured 81

ms, and the simulated shape of the acceleration profile, compared to the profile shown in Figure 5.5. The head maximum rotation of 2.86 degrees, obtained by twice integrating the subject head angular acceleration data, was also a primary criterion for evaluation of the simulated response.

The photogrammetric data of the Drop Tower Test (Figure 5.9) was used as a secondary criterion to evaluate the simulations. As shown in Chapter 5.1, maximum potential relative displacement between the subject's chest and mask was 1.1 inches in the Z-direction. The simulated head displacement response was compared to this value. Magnitudes of the maximum X and Y-direction accelerations and the times at which they were reached were also compared to measured data as a secondary evaluation criterion.

The simulation that was created using the original ATB characteristic for  $-G_x$  and  $G_y$  impact produced a response uncharacteristic of the measured human response to a  $10 G_z$  acceleration. The physical representation of model head response consisting of the contact ellipsoids for the head, neck, and torso segments is illustrated in Figure 6.1. This response shows full head rotation and chin-to-chest contact of the head and torso segment. The head segment Z-direction acceleration profile for the ATB head/neck model, shown in Figure 6.2 with overlaid measured head Z-direction

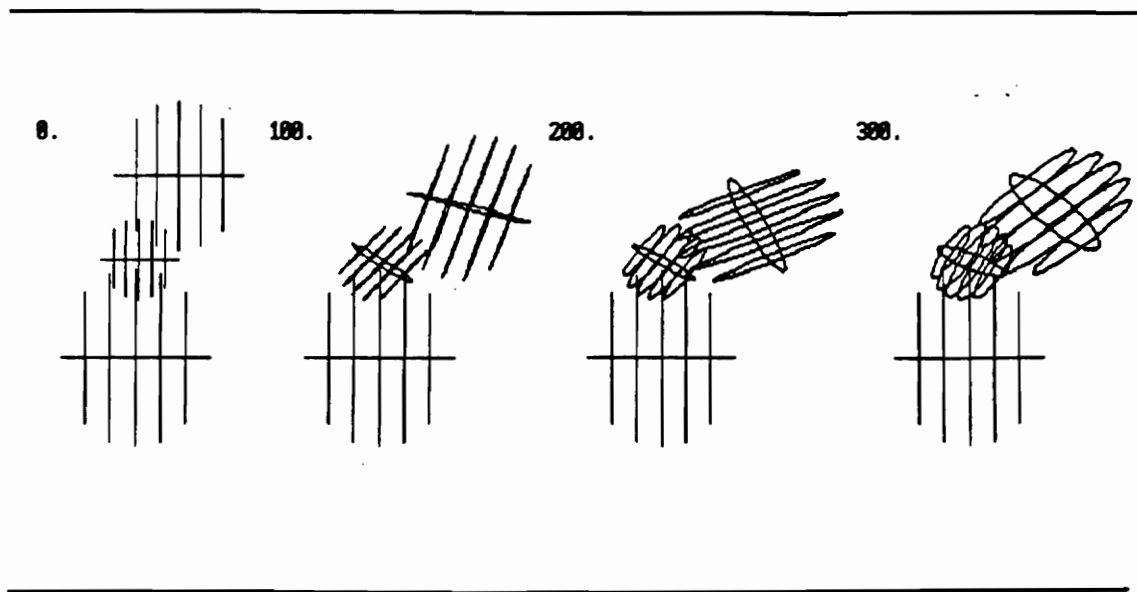


Figure 6.1 Response of Original ATB Head/Neck Model to 10  $G_z$  Acceleration



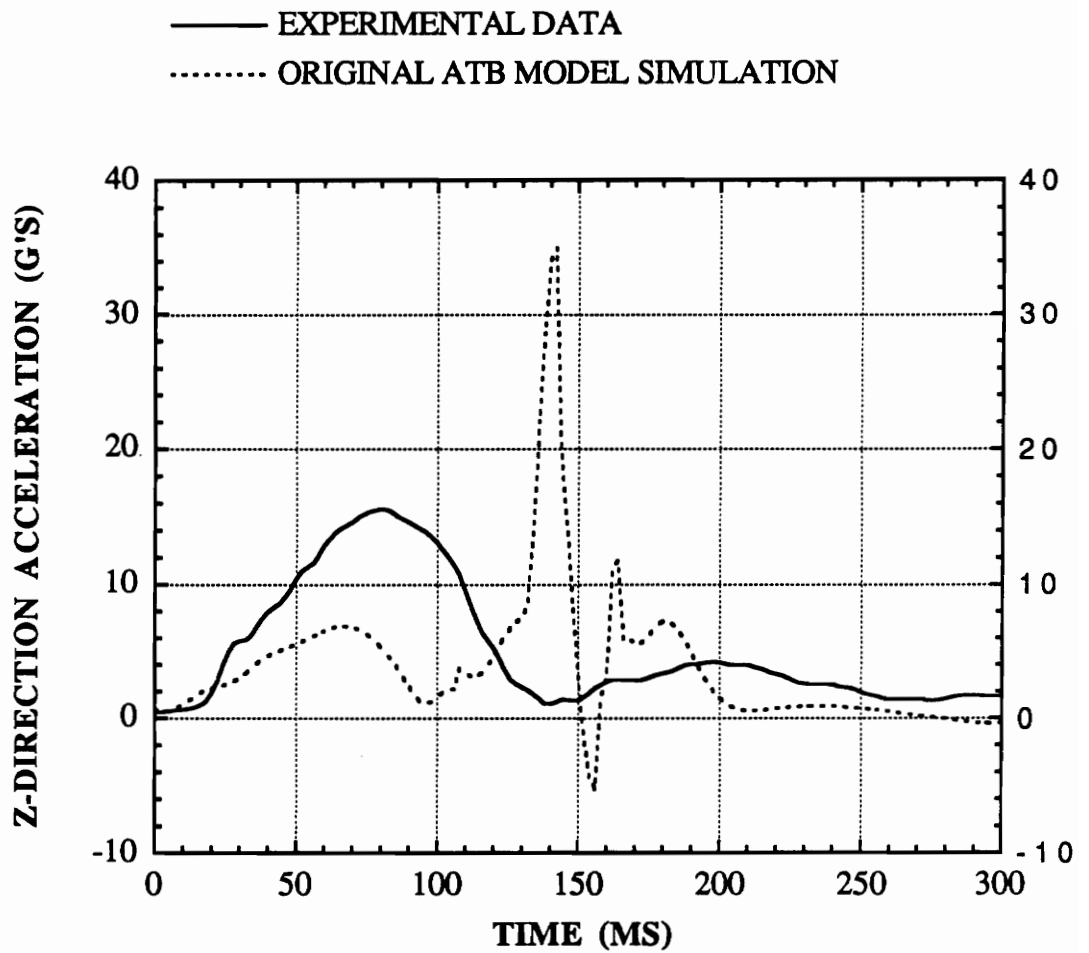


Figure 6.2 Comparison of Z-direction Head Acceleration  
During 10  $G_z$  Ejection from Experimental Data and  
Original ATB Model Simulation

acceleration data, is smooth from 0 to 100 ms, with a maximum acceleration of only 5.8 G at 66 ms as the head rotates forward. From 100 to 200 ms the Z-acceleration spikes to a maximum of 34 G's at 142 ms during the segment-segment contact; and from 200 to 300 ms the acceleration curve flattens out and approaches zero as the head rotates back upright. The maximum head rotation is 75.25 degrees, as compared to the 2.86 degrees measured for Subject L7.

In an attempt to reduce the amount of head rotation, increased restoring spring torques were applied to the upper and lower neck joints of the three segment/two ball and socket joint head/neck model. These torques simulated passive and/or active muscle and ligament resistance to rotation. This intermediate model included a modified linear spring coefficient for both joints of 150 lb/in (the subsequent spring coefficients from Table 5.1 were unchanged). The response, illustrated in Figure 6.3, shows rotation of the head in a bouncing manner. The head segment Z-direction acceleration for the head/neck model with the additional applied spring torques is shown in Figure 6.4 overlaid with the measured head Z-direction acceleration. The profile of this acceleration curve is similar to the measured acceleration profile. However, the maximum acceleration reached only 12.04 G's at 76 ms. This response is 77% of the target 15.66 G's measured head acceleration and is reached 5

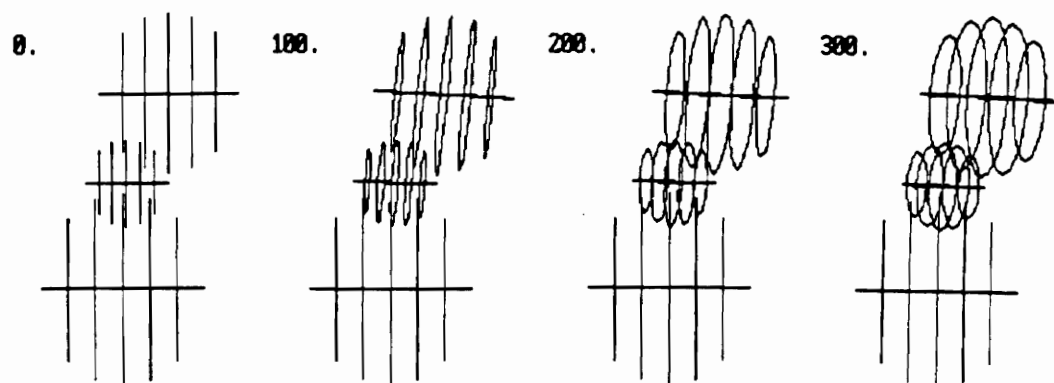


Figure 6.3 Response of Modified ATB Head/Neck Model to 10  $G_z$  Acceleration

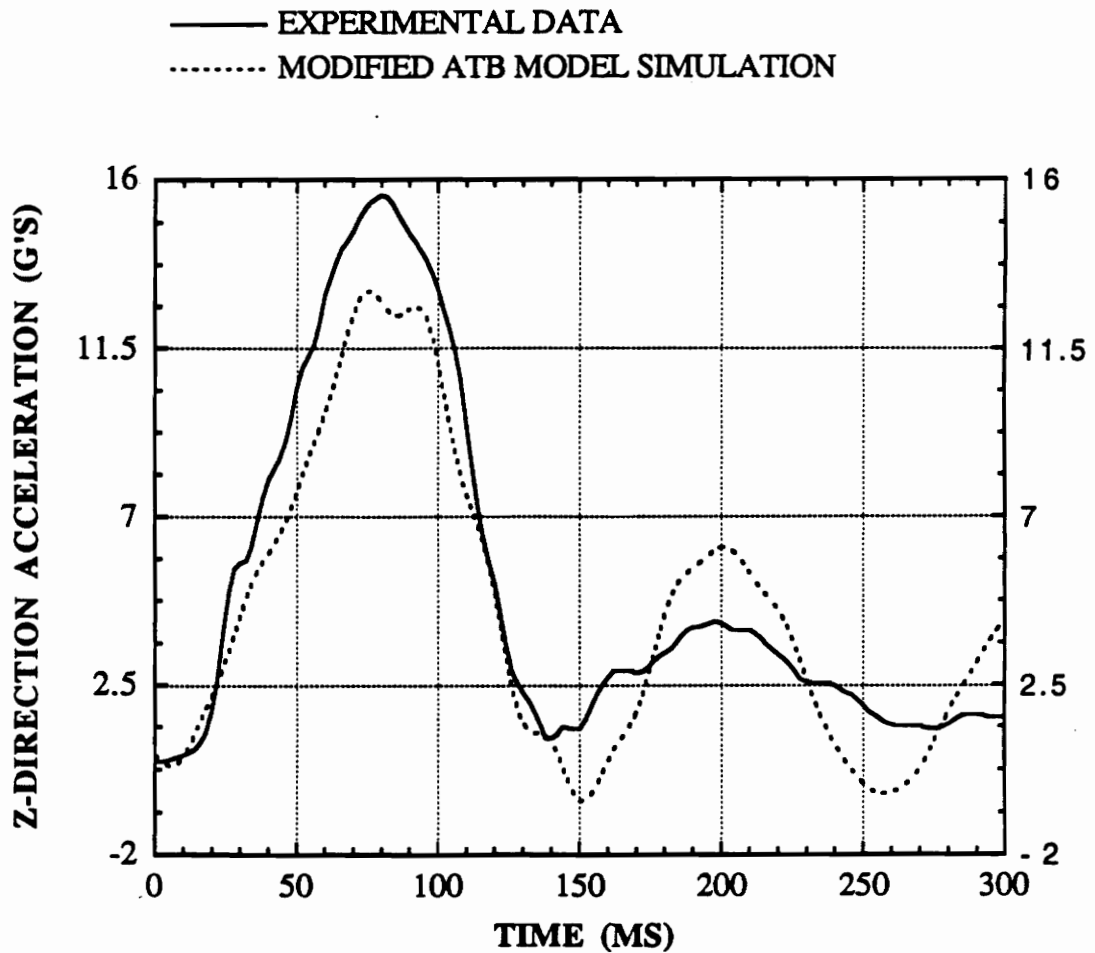


Figure 6.4 Comparison of Z-direction Head Acceleration During 10  $G_z$  Ejection from Experimental Data and Modified ATB Model Simulation

ms out of phase with the measured response. The head segment rotates 4.45 degrees before bouncing, which is more than one and a half times the measured maximum head rotation.

Increasing the spring torque further, while reducing the head rotation, was ineffective in increasing the Z-direction head acceleration. Thus, this model was replaced with the previously described slip joint model. A spring and viscous damper were used to characterize the slip joint resistance to motion to control the amount and rate of joint displacement. Since the test subject response mechanism shows the dominating response of the head and neck system to be head displacement in the Z direction, the effect of head and neck rotation was removed from the model by locking the joints to relative segment angular motion.

Simulations were performed with spring and damping coefficients described in Chapter 5.3 (Table 5.3). The simulation using a damping coefficient of 1.5 lb-sec/in and linear and quadratic spring coefficients of 50 lbs/in and 100 lbs/in<sup>2</sup>, respectively, produced a dynamic response to the +10 G acceleration closest to the test response of Subject L7. The response mechanism in Figure 6.5 shows linear head displacement similar to that described for the subject, and none of the head rotation seen in the original ATB simulation. The head segment Z-direction acceleration is plotted in Figure

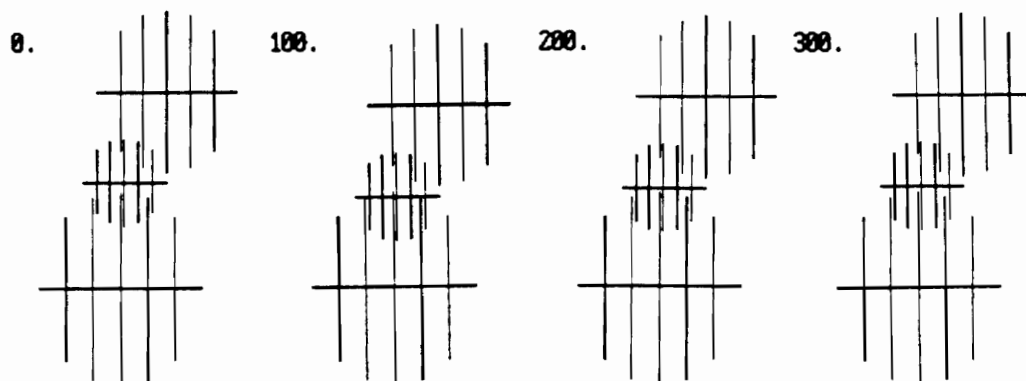


Figure 6.5 Response of Viscoelastic ATB Head/Neck  
Model to 10 G<sub>z</sub> Acceleration

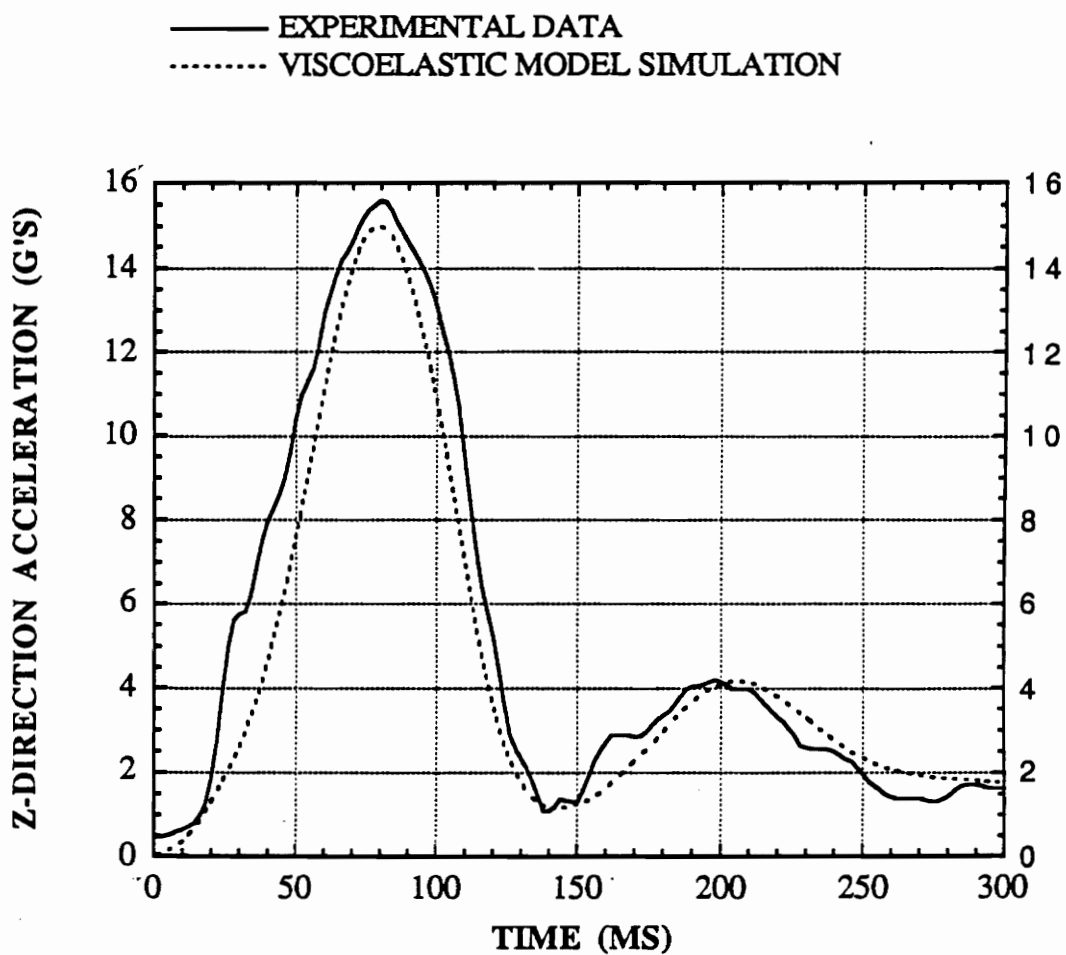


Figure 6.6 Comparison of Z-direction Head Acceleration During 10 G<sub>z</sub> Ejection from Experimental Data and Viscoelastic ATB Model Simulation

6.6, overlaid with the measured head Z-direction acceleration. The curves have similar profiles with the most notable difference being the widths of the large acceleration response regions between 0 and 120 ms. There is clear evidence in the response observed in the experimental data that suggests active muscle contraction initiated by the test subject at about 30 ms into the experiment influences the subsequent acceleration profile that is measured. The maximum head segment Z-direction acceleration is 15.01 G's at 80 ms, which is 95.85% of the target measured acceleration response and only 1 ms out of phase with it. Since this model was constrained from rotation, the segment head rotation was zero compared to the 2.8 degrees measured head rotation.

For the viscoelastic head/neck model, magnitude and occurrence time of maximum linear relative head displacement was a criterion for simulation evaluation. The photogrammetric data shown in Chapter 5.1 shows the approximate maximum mask displacement relative to the chest to be 1.1 inches. The maximum head segment displacement was 1.2 inches.



## 7.0 Summary and Conclusions

### 7.1 Modeling of the Head and Neck

Computer simulations of human dynamic response to acceleration were performed using three different characteristics to represent the properties of the human head and neck system. The first model was the original three rigid segment/two ball-and-socket joint head/neck analog. This simple analog did not allow relative "sliding" between segments, and restricted rotation at the joints by applying resistive torques to simulate muscle and ligament constraints in amounts currently deemed correct for human response. The same simple analog was used in the second model, but the amount of resistive torque applied to the joints was modified in an attempt to improve the predicted human response to experimentally measured acceleration. The third model was also a three segment model with a ball-and socket joint at the head/neck articulation. However, the neck/torso articulation was replaced by a "slip" joint. Joint rotation was not allowed in this model, and the sliding was controlled by spring and damper force elements.

The results of these simulations are presented in Figures 6.2, 6.4, and 6.6. The original ATB head/neck model composed of three segments and two ball-and-socket joints shows a profile which is uncharacteristic of the measured human profile. The addition of passive muscle and ligament constraints, modeled as increased resistive torques applied to the joints, was insufficient to improve the simulations significantly. Based on the response mechanism, as seen in photographic films, which showed no significant head rotation, a viscoelastic compression characteristic was used to improve the correlation between simulated head response and measured response to within a 4.1% difference in the maximum Z-direction acceleration.

Based on these observations, it is evident that the original neck characterization was insufficient for producing simulations which properly predict human head and neck response to ejection environments. As the test data of human response to 10 G acceleration acquired at the Armstrong Laboratory demonstrates, the amount of viscoelastic compression that occurs in the human pilot response to ejection is a significant factor in head response. Therefore, to adequately model the head/neck system of a live human subject, this effect must be incorporated into the head/neck characteristic used in the ATB model.

## 7.2 Direction of Future Studies

It has been demonstrated that the axial viscoelastic component of neck behavior must be considered when modeling the head/neck response to ejection accelerations. A number of steps must be taken before this approach can be used in practical predictive simulations for whole body response exposures.

Average spring and damping characteristics governing the viscoelastic sliding of the neck along the torso must be determined for typical air crew personnel. This can be accomplished by performing the iterative coefficient optimization procedure, described in Chapter 5.3 for subject L7, on the remainder of the subject data obtained in the Night Vision Goggle study at the Armstrong Laboratory.

For the model to be of sufficient flexibility for application to both  $G_z$  and  $G_x$  simultaneous accelerations, head rotational freedom must be reintroduced into the model and appropriate joint stops and stop characteristics must be applied. The inclusion of an active muscle element will also be necessary to produce predictive responses to lower  $G$  accelerations where voluntary muscle effect is apparent. The complexity of the cervical spine and its role in producing

head response necessitates an analog which models rotation, bending, and active and passive muscle response.

## 8.0 References

- (1) Guill, F.C. and Herd, G.R., "Aircrew Neck Injuries; A New, or an Existing, Misunderstood Phenomenon?", in: *Neck Injury in Advanced Military Aircraft Environments*, AGARD Conference Proceedings No. 471, pp. 9.1-12, 1990.
- (2) Rash, C.E., Verona, R.W., Crowley, J.S., "Human Factors and Safety Considerations of Night Vision Systems Flight Using Thermal Imaging Systems", USAARL Report No. 90-10, 1990.
- (3) Knox, F.S., Buhrman, J.R., Perry, C.E., Kaleps, I.; "Interim Head/Neck Criterion", Armstrong Laboratory Consultation Report, Wright-Patterson AFB, OH., Dec, 1991.
- (4) Obergefell, L.A., Gardner, T.R., Kaleps, I., and Fleck, J.T., "Articulated Total Body Model Enhancements", Vol 2. Armstrong Laboratory Tech Report, AAMRL-TR-88-043, Wright Patterson AFB, OH., 1988.
- (5) Fleck, J.T., "Calspan Three-Dimensional Crash Victim Simulation Program," *Aircraft Crashworthiness*, University Press of Virginia, 1975.
- (6) Kaleps, I., "Prediction of Whole Body Response to Impact Forces in Flight Environments," Edited by: von Gierke, H.E., AGARD Conf. Proc. No. 253, A1-14, 1978.
- (7) Frisch, G.D., Cooper, C., "Mathematical Modeling of the Head and Neck Response to  $-G_x$  Impact Acceleration (Minimum Articulation Requirements)" *Aviat., Space, Environ. Med.*, pp. 196-210, Jan. 1978.
- (8) Becker, E.B., "Preliminary Discussion of an Approach to Modeling Living Human Head and Neck to  $-G_x$  Impact Acceleration," in: King, W.F., and Mertz, H.J. Eds., *Human Impact Response, Measurement and Simulation*, Plenum Press, NY, 1973.
- (9) Freivalds, A., and Kaleps, I., "Computer-Aided Strength Prediction Using the Articulated Total Body Model." *Comput. and Indus. Engng.*, Vol. 8, No. 2, pp. 107-118, Pergamon Press Ltd., 1984.

- (10) Freivalds, A., McCauley, D.S., "Biodynamic Simulations of Helmet Mass and Center of Gravity Effects," *Journal of Safety Research*, Vol. 21, pp 141-148, National Safety Council and Pergamon Press, 1990.
- (11) Fleck, J.T., Butler, F.E., Vogel, S.L., "An Improved Three-Dimensional Computer Simulation of Motor Vehical Crash Victims," Calspan Corp. Tech Report, ZQ-5180-L-1, NY, 1974.
- (12) Jacob, S.W., Francone, C.A., and Lossow, W.J., *Structure and Function in Man*, Phila., PA, W.B. Saunders Co., 1982.
- (13) Grey, Henry, *Anatomy, Descriptive and Surgical*, NY, Bounty Books, 1977.
- (14) Heulke, D.F., "Anatomy of the Human Cervical Spine and Associated Structures," *The Human Neck-Anatomy, Injury Mechanisms, and Biomechanics*, Society of Automotive Engineers Inc., PA, 1979.
- (15) Schneck, D.J., *Mechanics of Muscle: Second Edition*, New York University Press, NY, 1992.
- (16) Weber, R.C., "An introduction to the elements of linear biomechanical modeling," in: Ewing, C.L., Thomas, D.J., Sances, A., Jr., and Larson, S.J., Eds., *Impact Injury of the Head and Spine*, Springfield, Ill., Charles C. Thomas, pp. 391-420, 1983.
- (17) Perry, C.E., "Test Plan for Evaluation of the Effects of Night Vision Goggles on Human Response During +G Impact Accelerations." AAMRL/BBP Office Report, Workunit 72313101, Aug, 1989.
- (18) Frisch, G.D., D'Aulerio, L. and O'Rourke, J., "Mechanism of head neck response to  $-G_x$  impact acceleration: a math modeling approach," *Aviat., Space, Environ. Med.*, 48(3): pp. 223-230, 1977.
- (19) Smith, D.E. and Anderson, W. R., "Predictive model of dynamic response of the human head/neck system to  $-G_x$  impact acceleration," *Aviat., Space, Environ. Med.*, 49(1): pp. 224-233, 1978.
- (20) Vulcan, A.P. and King, A.I., "Forces and Moments Sustained by the Lower Vertebral Column of a Seated Human During Seat to Head Acceleration" in: *Dynamic Response of Biomedical Systems*, NY, ASME, 1970, pp. 84-100.

- (21) Vulcan, A.P., King, A.I., and Nakamura, G.S., "Effects of bending on the vertebral column of seated human during seat-to-head acceleration", *Aerosp. Med.*, 41: 294, 1970.
- (22) Privitzer, E., and Kaleps, I., "Effects of Head Mounted Devices on Head-Neck Dynamic Response to +G<sub>z</sub> Accelerations", in: *Neck Injury in Advanced Military Aircraft Environments*, AGARD Conference Proceedings No. 471, pp. 13.1-14, 1990.
- (23) Belytschko, T., Rencis, M., Williams, J., "Enhancements to Secondary Loading Path Model and Validation of Head-Cervical Spine Model", Armstrong Laboratory Tech Report, AAMRL-TR-85-019, Wright Patterson AFB, OH, 1985.
- (24) Payne, P.R., "Injury potential of ejection seat cushions," *J. Aircr.*, 6: 273, 1969.
- (25) Yoganandan, N., Myklebust, J.B., Ray, G., and Sances, A. Jr., "Mathematical and Finite Element Analysis of Spine Injuries", *CRC Crit. Rev. in Biomed. Engr.*, 15(1): 29, 1987.
- (26) Von Gierke, H.E., Kaleps, I., "Biodynamic Motion and Injury Prediction" in: *Rev. Port. Med. Mil.*, 33(1), 1985.

# Appendix A

## Transformation of measured inertial tensor from anatomical coordinates to ATB local head segment coordinates

1) Given Combined Inertial Tensor (lb-in<sup>2</sup>) in anatomical

$$I_A = \begin{bmatrix} 144.07 & -2.9 & 9.73 \\ -2.9 & 149.09 & 1.2 \\ 9.73 & 1.2 & 120.1 \end{bmatrix}$$

coordinates:

Neglecting small products of inertia,  $I_A$  simplifies to:

$$I_A = \begin{bmatrix} 144.07 & 0.0 & 9.73 \\ 0.0 & 149.09 & 0.0 \\ 9.73 & 0.0 & 120.1 \end{bmatrix}$$

2) Translation from anatomical origin to measured location of combined head/helmet center of gravity:

measured cg distance (in):

$$\bar{x} = -0.1350 \quad \bar{y} = 0.0634 \quad \bar{z} = 0.9115$$

combined mass (lb):

$$m = 13.06$$



Neglecting lateral shift less than 0.1 inch, cg distance:

$$\bar{X} = -0.1350 \quad \bar{Y} = 0.0 \quad \bar{Z} = 0.9115$$

For moments of inertia ( $I_{XX}$ ,  $I_{YY}$ ,  $I_{ZZ}$ ):

$$\bar{I} = I - md^2 \quad [A1-1]$$

where

$\bar{I}$  is the moment of inertia at the center of mass,  
 $I$  is the given moment of inertia, and  
 $d^2$  is the distance between the old and new axes.

For products of inertia:

$$\begin{aligned} I_{XY} &= I_{YX} = \bar{I}_{XY} - m \bar{X} \bar{Y} \\ I_{YZ} &= I_{ZY} = \bar{I}_{YZ} - m \bar{Y} \bar{Z} \\ I_{XZ} &= I_{ZX} = \bar{I}_{XZ} - m \bar{X} \bar{Z} \end{aligned} \quad [A1-2]$$

The combined inertial tensor translated to the head/helmet center of gravity:

$$\bar{I}_A = \begin{bmatrix} 133.21 & 0.0 & 8.124 \\ 0.0 & 138.0 & 0.0 \\ 8.124 & 0.0 & 119.86 \end{bmatrix}$$

3) Rotation from anatomical orientation to local segment orientation:

$$\uparrow_{-x}^z \quad \text{anatomical} \qquad \downarrow_z^x \quad \text{local}$$

rotation about x-axis,

$$\theta = 180^\circ$$

Direction Cosine Matrix C:

$$C = \begin{bmatrix} 1 & 0 & 0 \\ 0 & \cos\theta & \sin\theta \\ 0 & -\sin\theta & \cos\theta \end{bmatrix}$$

Local inertial tensor  $\overline{I}_L$ :

$$\overline{I}_L = C \overline{I} C^T \quad [A1-3]$$

where the superscript T denotes the transpose of the matrix.

Measured inertial tensor translated and rotated to the head segment local coordinate system:

$$\overline{I}_L = \begin{bmatrix} 133.21 & 0.0 & -8.124 \\ 0.0 & 138.0 & 0.0 \\ -8.124 & 0.0 & 119.86 \end{bmatrix}$$

4) Calculation of principle moments of inertia:

$$A = \bar{\lambda} I \quad \text{general} \quad [\text{A1-4}]$$

$$\bar{I}_L = \bar{\lambda} I \quad \text{this case} \quad [\text{A1-5}]$$

where

$$I \text{ is the identity matrix, } \begin{bmatrix} 1 & 0 & 0 \\ 0 & 1 & 0 \\ 0 & 0 & 1 \end{bmatrix} \text{ and,}$$

$\bar{\lambda}$  is the eigenvector (equal to the principle moments  $\bar{I}_p$ )

Calculated principal moments of inertia in head segment local coordinates:

$$\bar{\lambda} = \begin{Bmatrix} 138.006 \\ 116.024 \\ 137.058 \end{Bmatrix} \quad (\text{lbm-in}^2)$$

In ATB units:

$$\bar{I}_p = \bar{\lambda} = \begin{Bmatrix} 0.355 \\ 0.356 \\ 0.301 \end{Bmatrix} \quad (\text{lb-in-sec}^2)$$

5) Calculation of direction cosines

$$\bar{I}_L \vec{X} = \lambda \vec{X} \quad [A1-6]$$

where the normalized x vector, calculated for each principle moment, generates the rows of the direction cosine matrix C of the principle moments of inertia in the head segment local coordinate system:

$$C = \begin{bmatrix} x_1^T \\ x_2^T \\ x_3^T \end{bmatrix} = \begin{bmatrix} 0.904 & 0.0 & -0.427 \\ 0 & 1 & 0 \\ 0.427 & 0 & 0.904 \end{bmatrix} \quad [A1-7]$$

where  $x_j^T$  is the transpose of the solution of [A1-6] for the jth eigenvalue

thus, rotation about the y-axis,  $\theta = 25.3^\circ$

# Appendix B

Execution of program ATB and program Dynaman (PC version of ATB model) to produce the viscoelastic slip joint

1) Designate the neck/torso joint to be a slip joint locked to angular rotation and unlocked to linear displacement:

## ATB Model:

- In the input file Card B3a:
  - define IPIN to be -5 and ISLIP to be -1

## DYNAMAN Program:

- In the INPUT PREPROCESSOR, under menu heading SEGMENT, sub-menu JOINT TYPE & LOCATION, choice JOINT DEFINITION:
  - highlight the section under JOINT TYPE corresponding to JOINT NP (neck joint), toggle the space bar to choose SLIP, press enter
  - highlight the section under LOCKED corresponding to JOINT NP, toggle the space bar to choose YES, press F10 to accept
  - highlight the section under SLP LOCK corresponding to JOINT NP, toggle to NO, press F10 to accept

2) Attach a quadratic spring and linear damper to the segments at the joint location

ATB Model:

- In the input file Card D1
  - Define NSD to be 1
- In the input file Card D8
  - Define MSDM to be 1 (torso)
  - Define MSDN to be 2 (neck)
  - Define APSDM to be the neck/torso joint location in the torso local coordinates
  - Define APSDN to be the neck/torso joint location in the neck local coordinates
  - Define ASD(1-5):
    - ASD(1) (D0) is 0
    - ASD(2) (A1) is the positive linear spring coefficient (lb/in)
    - ASD(3) (A2) is the quadratic spring coefficient (lb/in<sup>2</sup>)
    - ASD(4) (B1) is the linear damping coefficient (lb-sec/in)
    - ASD(5) (B2) is an optional quadratic damping

coefficient (lb-sec<sup>2</sup>/in<sup>2</sup>)

DYNAMAN Program:

- In the INPUT PREPROCESSOR, under menu ENVIRONMENT, sub-menu SPRING-DAMPERS
  - Choose (highlight/toggle/enter) UT (upper torso) for SEGMENT M and NECK for SEGMENT M
  - Enter the ASD coefficients described for the ATB model for the subsequent 5 coefficients and press enter
  - Enter the joint location in the corresponding local coordinate system where indicated

The five ASD coefficients are used in the SPDAMP subroutine to calculate the forces FS and FD:

$$FS = (D-DO) * (|A1| + A2 * |D-DO|) \quad [A2-1]$$

and

$$FD = DV * (B1 + B2 * |DV|) \quad [A2-2]$$

where D and DV are the distance and its time derivative between the spring-damper points of attachment APSDM and APSDN. These forces are considered external forces which are returned to the subroutine CONTCT which controls the subroutines required to compute external forces and torques acting on the body segments.

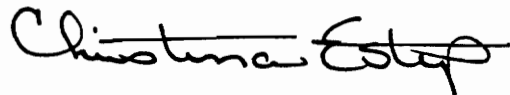
|    |  |                     |
|----|--|---------------------|
|    | SUBROUTINE SPDAMP  | SPDAMP              |
|    |  | REV IV 07/24/86SLIP |
| C  | COMPUTES THE SPRING AND VISCOUS FORCE OF A SPRING DAMPER BETWEEN   | SPDAMP              |
| C  | SPECIFIED POINTS ON SELECTED SEGMENTS AND ADDS THE RESULTING       | SPDAMP              |
| C  | FORCE AND TORQUE TO THE U1 AND U2 ARRAYS.                          | SPDAMP              |
| C  |  | SPDAMP              |
|    | IMPLICIT REAL*8(A-H,O-Z)   | SPDAMP              |
|    | COMMON/CONTRL/ TIME,NSEG,NJNT,NPL,NBLT,NBAG,NVEH,NGRND,            | SPDAMP              |
|    | * NS,NQ,NSD,NFLX,NHRNSS,NWINDF,NJNTF,NPRT(36),NPG                  | PAGE                |
|    | COMMON/SGMNTS/ D(3,3,30),WMEG(3,30),WMEGD(3,30),U1(3,30),U2(3,30), | SPDAMP              |
|    | * SEGLP(3,30),SEGLV(3,30),SEGLA(3,30),NSYM(30)                     | SPDAMP              |
|    | COMMON/DAMPER/ APSDM(3,20),APSDN(3,20),ASD(5,20),MSDM(20),MSDN(20) | SPDAMP              |
|    | COMMON/TABLES/MXNTI,MXNTB,MXTB1,MXTB2,NTI(50),NTAB(1250),TAB(4500) | BUTLER2             |
|    | COMMON/FORCES/PSF(7,70),BSF(4,20),SSF(10,40),BAGSF(3,20),          | NCFORC              |
|    | * PRJNT(7,30),NPANEL(5),NPSF,NBSF,NSSF,NBGSF                       | SPDAMP              |
|    | COMMON/TEMPVS/DELM(3),DELN(3),DD(3),DEL,T1(3),T2(3),T3(3),T4(3),   | SPDAMP              |
|    | * DUNIT(3),DV(3),DMV,DDO,FS,FD,TOTF(3),                            | SPDAMP              |
|    | * T5(3),T6(3),T7(3),T8(3)  | SPDAMP              |
|    | CALL ELTIME(1,32)  | SPDAMP              |
|    | NBSFO = NBSF   | SPDAMP              |
|    | DO 90 I=1,NSD  | SPDAMP              |
|    | M = MSDM(I)  | SPDAMP              |
|    | N = MSDN(I)  | SPDAMP              |
| C  |  | SPDAMP              |
| C  | COMPUTE VECTOR AND ITS MAGNITUDE BETWEEN THE SPECIFIED POINTS.     | SPDAMP              |
| C  |  | SPDAMP              |
|    | CALL DOT31 (D(1,1,M),APSDM(1,I),DELM)                              | SPDAMP              |
|    | CALL DOT31 (D(1,1,N),APSDN(1,I),DELN)                              | SPDAMP              |
|    | DEL = 0.0  | SPDAMP              |
|    | DO 10 K=1,3  | SPDAMP              |
|    | DD(K) = SEGLP(K,M)+DELM(K)-SEGLP(K,N)-DELN(K)                      | SPDAMP              |
| 10 | DEL = DEL+DD(K)**2   | SPDAMP              |
|    | IF (DEL.LE.0.0) GO TO 90   | SPDAMP              |
|    | DEL = DSQRT(DEL)   | SPDAMP              |
| C  |  | SPDAMP              |
| C  | COMPUTE RELATIVE VELOCITY AND ITS COMPONENT ON VECTOR LINE.        | SPDAMP              |
| C  |  | SPDAMP              |
|    | CALL CROSS(WMEG(1,M),APSDM(1,I),T1)                                | SPDAMP              |
|    | CALL CROSS(WMEG(1,N),APSDN(1,I),T2)                                | SPDAMP              |
|    | CALL DOT31 (D(1,1,M),T1,T3)  | SPDAMP              |
|    | CALL DOT31 (D(1,1,N),T2,T4)  | SPDAMP              |
|    | DO 20 K=1,3  | SPDAMP              |
|    | DUNIT(K) = DD(K)/DEL   | SPDAMP              |
| 20 | DV(K) = SEGLV(K,M)+T3(K)-SEGLV(K,N)-T4(K)                          | SPDAMP              |
|    | DMV = DUNIT(1)*DV(1)+DUNIT(2)*DV(2)+DUNIT(3)*DV(3)                 | SPDAMP              |
| C  |  | SPDAMP              |
| C  | COMPUTE SPRING AND VISCOUS FORCE AND THE COMPONENTS                | SPDAMP              |
| C  | ALONG THE UNIT VECTOR  | SPDAMP              |
| C  |  | SPDAMP              |
|    | FS = 0.0   | SPDAMP              |



|   |        |
|---|--------|
| FD = 0.0  | SPDA.  |
| IF (ASD(1,I).LT.0.0) GO TO 21                                     | SLIP   |
| DDO = DEL-ASD(1,I)  | SPDAI  |
| IF (DDO.LE.0.0 .AND. ASD(2,I).LE.0.0) GO TO 41                    | SPDAI  |
| FS = DDO*(DABS(ASD(2,I)) + DABS(DDO)*ASD(3,I))                    | SPDAM  |
| FD = DMV*(ASD(4,I)+DABS(DMV)*ASD(5,I))                            | SPDAMP |
| GO TO 29  | SPDAMP |
| 21 DDO = DEL+ASD(1,I)   | SPDAMP |
| JF1 = ASD(2,I)  | SPDAMP |
| IF (JF1.EQ.0) GO TO 22  | SPDAMP |
| JF2 = NTI(JF1)  | SPDAMP |
| IF (DDO.GT.0.0 .OR. ASD(3,I).EQ.0.0) FS = EVALFD(DDO,JF2,1)       | SPDAMP |
| 22 JF3 = ASD(4,I)   | SPDAMP |
| IF (JF3.EQ.0) GO TO 29  | SPDAMP |
| JF4 = NTI(JF3)  | SPDAMP |
| IF (DDO.GT.0.0 .OR. ASD(3,I).EQ.0.0) FD = EVALFD(DMV,JF4,1)       | SLIP   |
| 29 DO 30 K=1,3  | SPDAMP |
| 30 TOTF(K) = (FS+FD)*DUNIT(K)                                     | SPDAMP |
| C   | SPDAMP |
| C AND ADD THE RESULTING FORCE AND TORQUE TO THE U1 AND U2 ARRAYS. | SPDAMP |
| C   | SPDAMP |
| CALL MAT31(D(1,1,M),TOTF,T5)                                      | SPDAMP |
| CALL MAT31(D(1,1,N),TOTF,T6)                                      | SPDAMP |
| CALL CROSS(APSDM(1,I),T5,T7)                                      | SPDAMP |
| CALL CROSS(APSDN(1,I),T6,T8)                                      | SPDAMP |
| DO 40 K=1,3   | SPDAMP |
| U1(K,M) = U1(K,M) - TOTF(K)                                       | SPDAMP |
| U1(K,N) = U1(K,N) + TOTF(K)                                       | SPDAMP |
| U2(K,M) = U2(K,M) - T7(K)   | SPDAMP |
| 40 U2(K,N) = U2(K,N) + T8(K)                                      | SPDAMP |
| 41 IBSF = 3-2*MOD(I,2)  | SPDAMP |
| NBSF = NBSFO + (I+1)/2  | SPDAMP |
| BSF(IBSF,NBSF) = DEL  | SPDAMP |
| BSF(IBSF+1,NBSF) = FD + FS  | SPDAMP |
| 90 CONTINUE   | SPDAMP |
| CALL ELTIME(2,32)   | SPDAMP |
| RETURN  | SPDAMP |
| END   | SPDAMP |

## Vita

The author, Christina R. Estep, was born on December 21, 1966 in Fairfax, VA. In May 1990, she obtained a Bachelor of Science Degree in Mechanical Engineering From Virginia Polytechnic Institute and State University. Since that time, she has been studying Biomechanical Engineering in the Engineering Science and Mechanics Department at VPI&SU. She studied Biodynamics during the Summers of 1991 and 1992 at the Armstrong Laboratory located at Wright-Patterson Air Force Base, Dayton, Ohio, as a Graduate Student Research Fellow of the Air Force Office of Scientific Research Summer Program.

A handwritten signature in black ink that reads "Christina Estep". The signature is written in a cursive style with a horizontal line underlining the first name.